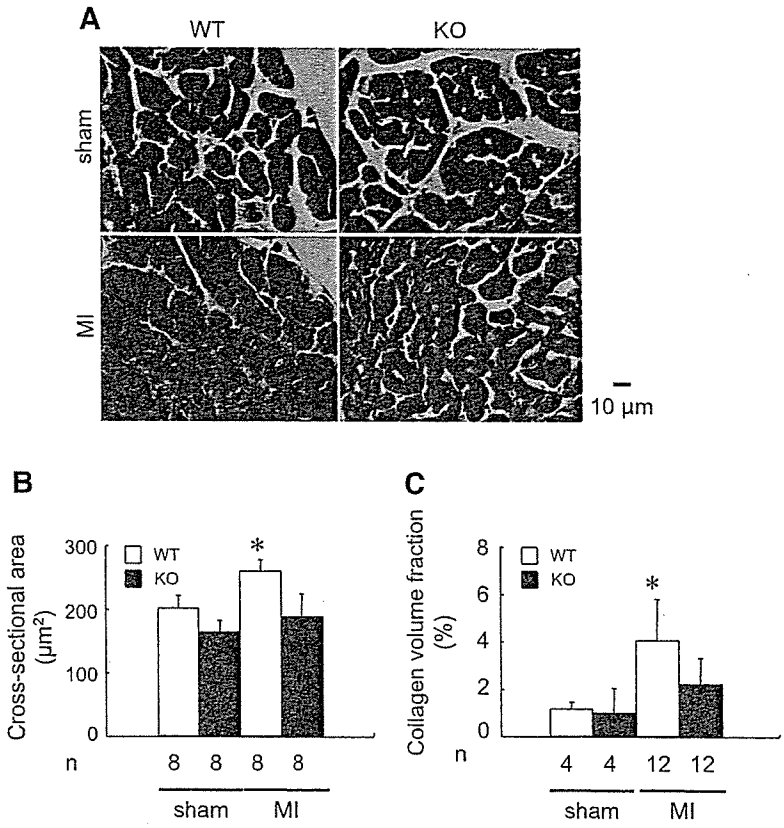

Fig. 3. Histology of noninfarct myocardium 4 wk after sham or left coronary artery ligation (MI). *A*: representative micrographs of Masson-trichrome staining for wild-type (WT) and NF-κB-KO mice. *B*: summarized data of cross-sectional area of cardiomyocytes. *C*: summarized data of collagen volume fraction. Values are means ± SD. $*P < 0.05$ vs. WT + sham operated.

DISCUSSION

In the present study, we investigated the role of NF-κB in the pathogenesis of cardiac remodeling and heart failure after MI. We confirmed that NF-κB was activated in noninfarct as well as infarct myocardium in WT + MI mice. Targeted disruption of the p50 subunit of NF-κB abrogated the activation of NF-κB and ameliorated myocyte hypertrophy, interstitial fibrosis, and cardiac dysfunction in KO + MI mice, indicating that cardiac remodeling and heart failure after MI is mediated by the activation of NF-κB. In contrast, induction of proinflammatory cytokines and chemokines was not ameliorated but rather enhanced in KO + MI mice, suggesting that myocardial inflammation after MI might be mediated by NF-κB-independent pathways. Although the precise mechanisms by which blockade of NF-κB ameliorated cardiac dysfunction and heart failure after MI remain undetermined, selective abrogation of JNK phosphorylation in KO mice might play an important role. These results indicate that blockade of NF-κB might be a new therapeutic strategy to prevent ventricular remodeling and heart failure after MI.

The role of NF-κB activation in acute myocardial ischemia remains controversial and might be different between transient and sustained myocardial ischemia. Studies using a model of ischemia-reperfusion injury have shown that blockade of NF-κB reduces infarct size and protects myocytes from ischemic insult (2, 15). In contrast, a study using a model of permanent coronary ligation has reported that blockade of NF-κB promotes myocyte apoptosis and increases infarct size 24 h after MI (14). However, the long-term effects of NF-κB blockade after permanent coronary ligation have not been investigated. In the present study, we used a MI model of permanent coronary ligation to evaluate the long-term effects of NF-κB blockade on ventricular remodeling and heart failure. Because we ligated the coronary artery carefully to ensure that the area at risk was consistent, the infarct size evaluated 4 wk after MI was not different between WT + MI and KO + MI mice. However, the rate of ventricular rupture was significantly different between WT + MI and KO + MI mice. All the ventricular ruptures occurred within 7 days after MI, and the incidence was twice higher in WT + MI mice. Because ventricular rupture may reflect an imbalance between myocardial death and repair, the reduction of ventricular rupture in KO + MI mice suggests that blockade of NF-κB might have retarded myocardial cell death and/or enhanced tissue repair and scar formation to maintain integrity of the infarct myocardium. Taken together, these results suggest that the net effect of NF-κB blockade is not harmful but desirable even after permanent occlusion of coronary arteries.

We have previously reported that blockade of NF-κB ameliorates myocardial hypertrophy in response to chronic infusion of ANG II (9) and improves cardiac function and survival in TNF-α-induced cardiomyopathy (8). In the present study, we have demonstrated that blockade of NF-κB improves cardiac function and survival after MI with

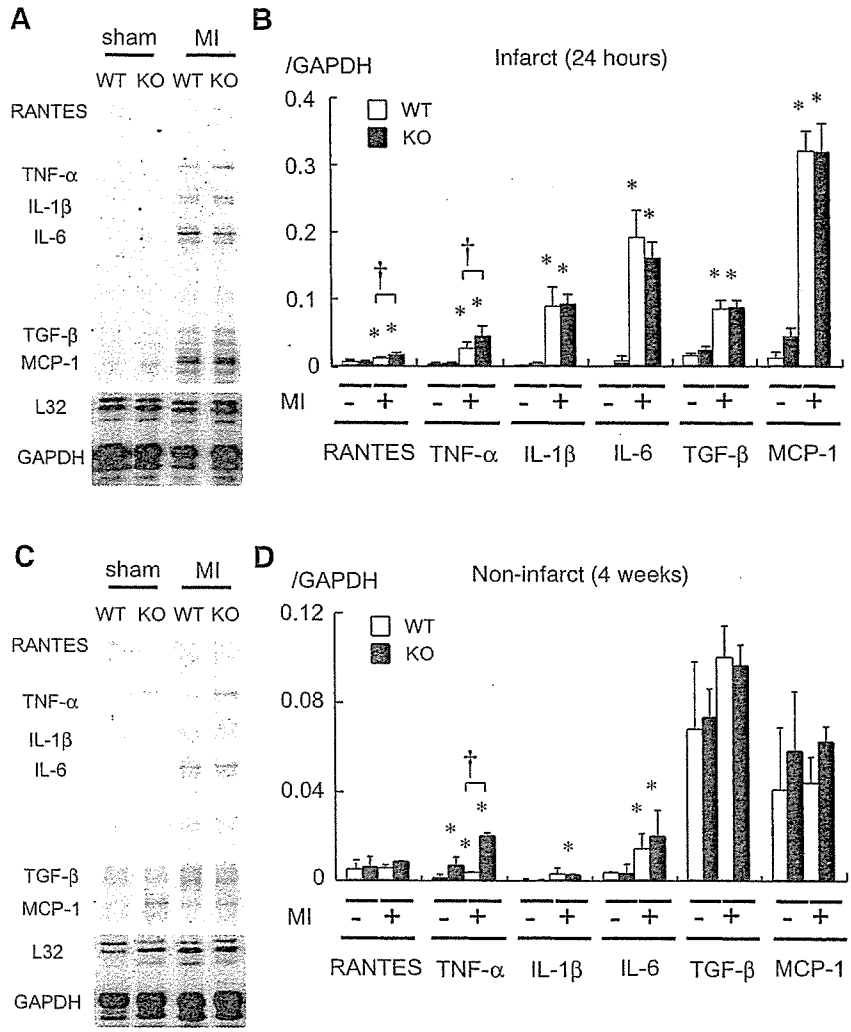

Fig. 4. Expression of proinflammatory cytokines and chemokines after MI. RNA was extracted from infarct myocardium 24 h after MI (*A*, *B*) and noninfarct myocardium 4 wk after MI (*C*, *D*) in WT and NF-κB-KO mice. Representative gels of multiprobe RNase protection assay (RPA) are shown in *A* and *C*, and summarized data are shown in *B* and *D*. The no. of animals are as follows: WT + sham operated (n = 3), KO + sham operated (n = 3), WT + MI (n = 5), KO + MI (n = 4) for infarct myocardium (*B*); WT + sham operated (n = 4), KO + sham operated (n = 5), WT + MI (n = 4), KO + MI (n = 3) for noninfarct myocardium (*D*). Values are means ± SD. TGF-β, transforming growth factor-β; RANTES, regulated on activation, normal T cell expressed and secreted; MCP-1, monocyte chemoattractant protein-1. *P < 0.05 vs. WT + sham operated, †P < 0.05 vs. WT + MI.

amelioration of myocyte hypertrophy and interstitial fibrosis. Although the precise mechanisms by which NF-κB promotes myocyte hypertrophy remain undetermined, it is of interest that phosphorylation of JNK was abrogated in p50-knockout mice. Because the protein level of JNK is not affected in p50-knockout mice, expression or activation of upstream kinases may be modulated by NF-κB pathways. MAP kinase signaling pathways, including ERK, JNK, and p38, are supposed to play an important role in cardiac hypertrophy and remodeling because they are phosphorylated and activated by G protein-coupled receptor agonists such as phenylephrine, endothelin-1, and ANG II (3, 21). Especially, JNK is also termed the stress-activated protein kinase because it is additionally activated by cellular stresses such as reactive oxygen species and proinflammatory cytokines, including IL-1β and TNF-α (21). Substrates of JNK are transcription factors, including c-Jun, ATF2, and Elk1 (21). Inhibition of JNK has been shown to abrogate ventricular hypertrophy in vivo in response to pressure overload (4) or $G_{\alpha}q$ overexpression (13). Therefore, the attenuated myocyte hypertrophy after MI in p50-knockout mice may be mediated by the abrogation of the JNK pathways.

Although activation of NF-κB has been shown to induce various proinflammatory cytokines and chemokines, including TNF-α (1), we have previously reported that expression of proinflammatory cytokines in response to chronic infusion of ANG II or TNF-α-induced cardiomyopathy was not abrogated by targeted disruption of the p50 subunit of NF-κB (8, 9). In the present study, expression of proinflammatory cytokines in infarct and noninfarct myocardium was not ameliorated but rather enhanced in KO + MI mice. These results suggest that expression of proinflammatory cytokines in the failing heart may be mediated by NF-κB-independent pathways. Because blockade of NF-κB improved cardiac function with amelioration of myocyte hypertrophy and interstitial fibrosis in KO + MI mice, myocardial expression of proinflammatory cytokines may not be harmful in the progression of ventricular remodeling and heart failure after MI unless NF-κB is activated.

The paradoxical increase of TNF-α and RANTES in KO + MI mice might be explained by the difference in tran-

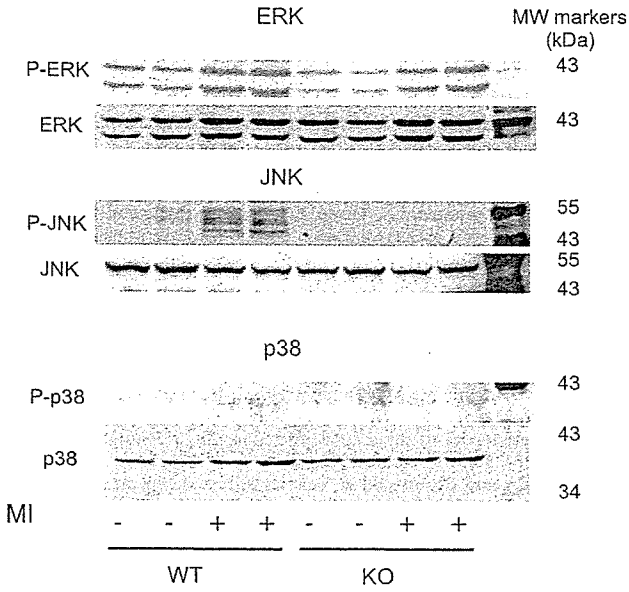

Fig. 5. Western blot analysis of ERK, JNK, and p38 with anti-phosphospecific (P-ERK, P-JNK, P-p38) or nonphosphospecific (ERK, JNK, p38) antibodies 7 days after MI. KO, NF-κB knockout mice.

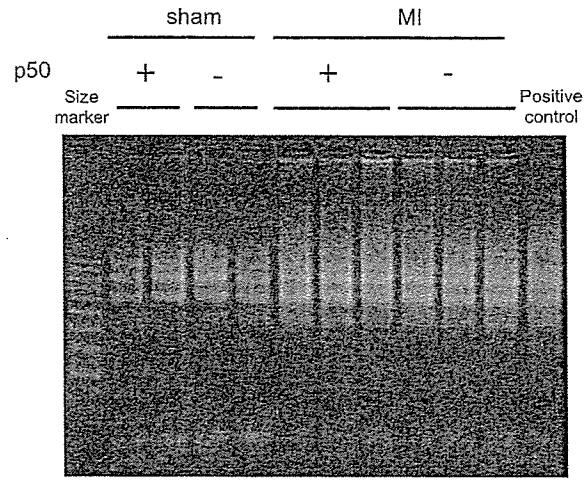

Fig. 6. Ligation-mediated PCR assay to demonstrate DNA laddering of samples prepared from sham-operated mice and infarct myocardium 24 h after MI.

scriptional activity of the p50-p65 heterodimer and p50-p50 homodimer (11). The NF-κB/Rel family consists of five subunit members: p50, p52, c-Rel, RelA (p65), and RelB. In most cells, NF-κB is a heterodimer of p50 and p65 that exists in the cytoplasm and is bound to the inhibitory protein IκB. Activation of NF-κB occurs when specific IκB kinases phosphorylate the IκB. After chronic exposure to proinflammatory cytokines, including TNF-α, NF-κB is converted from the transcriptionally active p50-p65 heterodimer to the transcriptionally inactive p50-p50 homodimer (6, 11), which may act as a native negative-feedback mechanism to prevent excessive inflammatory responses. The absence of p50-p50 homodimers in mice with targeted disruption of the p50 subunit therefore may account for enhanced expression of TNF-α and RANTES in KO + MI mice.

The cross-sectional area of cardiomyocytes in noninfarct myocardium was significantly increased in WT + MI mice. However, the wall thickness evaluated by echocardiography was not statistically different between WT + sham-operated and WT + MI mice. This might be explained as follows. Although the difference was not statistically significant, there was a trend of increased wall thickness in MI mice. The WT + MI to WT + sham-operated ratio of noninfarct wall thickness was 1.14/0.97 = 1.18. On the other hand, the cross-sectional area of myocyte in WT + MI mice was significantly greater than that in WT + sham-operated mice, with a ratio of 260/201 = 1.29. Because area is a two-dimensional parameter, the square root of cross-sectional area should correlate with wall thickness. Indeed, the square root of 1.29 is 1.14, which is close to the ratio of wall thickness of 1.18. Because the resolution of echocardiography is limited, it might not be able to consistently differentiate differences in thickness of <20%.

In the present study, to achieve complete and chronic inhibition of NF-κB in vivo, we used gene-manipulated mice lacking the p50 subunit of NF-κB. These mice show no developmental abnormalities but exhibit multifocal defects in B-cell-mediated immune responses and nonspecific responses to infection. In these animals, B cells do not proliferate in response to bacterial lipopolysaccharide and are defective in basal and specific antibody production (19). Although we did not detect any adverse effects or premature death in the p50-knockout mice during the observation period, systemic inhibition of NF-κB may be deleterious in the long run. Therefore, it may be desirable to employ cardiac-specific inhibition of NF-κB to minimize immunological detrimental effects. Furthermore, the results observed in gene-manipulated mice may be different from the outcomes of pharmacological interventions because an inherent deficit of a specific gene may alter the expression and functions of other genes as compensation mechanisms. Therefore, further studies are required to draw a final conclusion that blockade of NF-κB is beneficial and applicable as a therapeutic strategy for patients with MI.

Table 3. *Area at risk and infarct area 24 h after coronary ligation*

	WT + MI	KO + MI
n	5	6
Area at risk, %	39.7±2.98	37.9±2.68
Infarct area, %	20.6±2.80	14.9±2.21*
Infarct area/area at risk, %	52.1±5.90	39.4±6.96*

Data are means ± SD; *n* indicates no. of animals studied. *$P < 0.05$ vs. WT + MI.

GRANTS

A part of this study was conducted in Kyushu University Station for Collaborative Research. This study was supported by a grant from Kimura Memorial Heart Foundation, by the Grant for Research on Cardiovascular Disease from Japan Heart Foundation/Pfizer Pharmaceuticals, and by the Grant-in-Aid for Scientific Research from the Japan Society for the Promotion of Science (C15590755).

REFERENCES

1. **Barnes PJ and Karin M.** Nuclear factor-κB: a pivotal transcription factor in chronic inflammatory diseases. *N Engl J Med* 336: 1066–1071, 1997.
2. **Brown M, McGuinness M, Wright T, Ren X, Wang Y, Boivin GP, Hahn H, Feldman AM, and Jones WK.** Cardiac-specific blockade of NF-κB in cardiac pathophysiology: differences between acute and chronic stimuli in vivo. *Am J Physiol Heart Circ Physiol* 289: H466–H476, 2005.
3. **Bueno OF and Molkentin JD.** Involvement of extracellular signal-regulated kinases 1/2 in cardiac hypertrophy and cell death. *Circ Res* 91: 776–781, 2002.
4. **Choukroun G, Hajjar R, Fry S, del Monte F, Haq S, Guerrero JL, Picard M, Rosenzweig A, and Force T.** Regulation of cardiac hypertrophy in vivo by the stress-activated protein kinases/c-Jun NH_2-terminal kinases. *J Clin Invest* 104: 391–398, 1999.
5. **Grabellus F, Levkau B, Sokoll A, Welp H, Schmid C, Deng MC, Takeda A, Breithardt G, and Baba HA.** Reversible activation of nuclear factor-κB in human end-stage heart failure after left ventricular mechanical support. *Cardiovasc Res* 53: 124–130, 2002.
6. **Haudek SB, Bryant DD, and Giroir BP.** Differential regulation of myocardial NFκB following acute or chronic TNF-α exposure. *J Mol Cell Cardiol* 33: 1263–1271, 2001.
7. **Hirotani S, Otsu K, Nishida K, Higuchi Y, Morita T, Nakayama H, Yamaguchi O, Mano T, Matsumura Y, Ueno H, Tada M, and Hori M.** Involvement of nuclear factor-κB and apoptosis signal-regulating kinase 1 in G-protein-coupled receptor agonist-induced cardiomyocyte hypertrophy. *Circulation* 105: 509–515, 2002.
8. **Kawamura N, Kubota T, Kawano S, Monden Y, Feldman AM, Tsutsui H, Takeshita A, and Sunagawa K.** Blockade of NF-κB improves cardiac function and survival without affecting inflammation in TNF-α-induced cardiomyopathy. *Cardiovasc Res* 66: 520–529, 2005.
9. **Kawano S, Kubota T, Monden Y, Kawamura N, Tsutsui H, Takeshita A, and Sunagawa K.** Blockade of NF-κB ameliorates myocardial hypertrophy in response to chronic infusion of angiotensin II. *Cardiovasc Res* 67: 689–698, 2005.
10. **Kubota T, Miyagishima M, Alvarez RJ, Kormos R, Rosenblum WD, Demetris AJ, Semigran MJ, Dec GW, Holubkov R, McTiernan CF, Mann DL, Feldman AM, and McNamara DM.** Expression of proinflammatory cytokines in the failing human heart: comparison of recent-onset and end-stage congestive heart failure. *J Heart Lung Transplant* 19: 819–824, 2000.
11. **Lawrence T, Gilroy DW, Colville-Nash PR, and Willoughby DA.** Possible new role for NF-κB in the resolution of inflammation. *Nat Med* 7: 1291–1297, 2001.
12. **Li Y, Ha T, Gao X, Kelley J, Williams DL, Browder IW, Kao RL, and Li C.** NF-κB activation is required for the development of cardiac hypertrophy in vivo. *Am J Physiol Heart Circ Physiol* 287: H1712–H1720, 2004.
13. **Minamino T, Yujiri T, Terada N, Taffet GE, Michael LH, Johnson GL, and Schneider MD.** MEKK1 is essential for cardiac hypertrophy and dysfunction induced by Gq. *Proc Natl Acad Sci USA* 99: 3866–3871, 2002.
14. **Misra A, Haudek SB, Knuefermann P, Vallejo JG, Chen ZJ, Michael LH, Sivasubramanian N, Olson EN, Entman ML, and Mann DL.** Nuclear factor-κB protects the adult cardiac myocyte against ischemia-induced apoptosis in a murine model of acute myocardial infarction. *Circulation* 108: 3075–3078, 2003.
15. **Morishita R, Sugimoto T, Aoki M, Kida I, Tomita N, Moriguchi A, Maeda K, Sawa Y, Kaneda Y, Higaki J, and Ogihara T.** In vivo transfection of cis element "decoy" against nuclear factor-κB binding site prevents myocardial infarction. *Nat Med* 3: 894–899, 1997.
16. **Patten RD, Aronovitz MJ, Deras-Mejia L, Pandian NG, Hanak GG, Smith JJ, Mendelsohn ME, and Konstam MA.** Ventricular remodeling in a mouse model of myocardial infarction. *Am J Physiol Heart Circ Physiol* 274: H1812–H1820, 1998.
17. **Pfeffer MA and Braunwald E.** Ventricular remodeling after myocardial infarction. Experimental observations and clinical implications. *Circulation* 81: 1161–1172, 1990.
18. **Purcell NH, Tang G, Yu C, Mercurio F, DiDonato JA, and Lin A.** Activation of NF-κB is required for hypertrophic growth of primary rat neonatal ventricular cardiomyocytes. *Proc Natl Acad Sci USA* 98: 6668–6673, 2001.
19. **Sha WC, Liou HC, Tuomanen EI, and Baltimore D.** Targeted disruption of the p50 subunit of NF-κB leads to multifocal defects in immune responses. *Cell* 80: 321–330, 1995.
20. **Shiomi T, Tsutsui H, Matsusaka H, Murakami K, Hayashidani S, Ikeuchi M, Wen J, Kubota T, Utsumi H, and Takeshita A.** Overexpression of glutathione peroxidase prevents left ventricular remodeling and failure after myocardial infarction in mice. *Circulation* 109: 544–549, 2004.
21. **Sugden PH and Clerk A.** "Stress-responsive" mitogen-activated protein kinases (c-Jun N-terminal kinases and p38 mitogen-activated protein kinases) in the myocardium. *Circ Res* 83: 345–352, 1998.
22. **Torre-Amione G, Kapadia S, Lee J, Durand JB, Bies RD, Young JB, and Mann DL.** Tumor necrosis factor-α and tumor necrosis factor receptors in the failing human heart. *Circulation* 93: 704–711, 1996.
23. **Wong SC, Fukuchi M, Melnyk P, Rodger I, and Giaid A.** Induction of cyclooxygenase-2 and activation of nuclear factor-κB in myocardium of patients with congestive heart failure. *Circulation* 98: 100–103, 1998.

Overexpression of Mitochondrial Peroxiredoxin-3 Prevents Left Ventricular Remodeling and Failure After Myocardial Infarction in Mice

Shouji Matsushima, MD; Tomomi Ide, MD, PhD; Mayumi Yamato, PhD; Hidenori Matsusaka, MD; Fumiyuki Hattori, PhD; Masaki Ikeuchi, MD; Toru Kubota, MD, PhD; Kenji Sunagawa, MD, PhD; Yasuhiro Hasegawa, PhD; Tatsuya Kurihara, PhD; Shinzo Oikawa, PhD; Shintaro Kinugawa, MD, PhD; Hiroyuki Tsutsui, MD, PhD

Background—Mitochondrial oxidative stress and damage play major roles in the development and progression of left ventricular (LV) remodeling and failure after myocardial infarction (MI). We hypothesized that overexpression of the mitochondrial antioxidant, peroxiredoxin-3 (Prx-3), could attenuate this deleterious process.

Methods and Results—We created MI in 12- to 16-week-old, male Prx-3–transgenic mice (TG+MI, n=37) and nontransgenic wild-type mice (WT+MI, n=39) by ligating the left coronary artery. Prx-3 protein levels were 1.8 times higher in the hearts from TG than WT mice, with no significant changes in other antioxidant enzymes. At 4 weeks after MI, LV thiobarbituric acid–reactive substances in the mitochondria were significantly lower in TG+MI than in WT+MI mice (mean±SEM, 1.5±0.2 vs 2.2±0.2 nmol/mg protein; n=8 each, $P<0.05$). LV cavity dilatation and dysfunction were attenuated in TG+MI compared with WT+MI mice, with no significant differences in infarct size (56±1% vs 55±1%; n=6 each, P=NS) and aortic pressure between groups. Mean LV end-diastolic pressures and lung weights in TG+MI mice were also larger than those in WT+sham-operated mice but smaller than those in WT+MI mice. Improvement in LV function in TG+MI mice was accompanied by a decrease in myocyte hypertrophy, interstitial fibrosis, and apoptosis in the noninfarcted LV. Mitochondrial DNA copy number and complex enzyme activities were significantly decreased in WT+MI mice, and this decrease was also ameliorated in TG+MI mice.

Conclusions—Overexpression of Prx-3 inhibited LV remodeling and failure after MI. Therapies designed to interfere with mitochondrial oxidative stress including the antioxidant Prx-3 might be beneficial in preventing cardiac failure. (***Circulation*. 2006;113:1779-1786.**)

Key Words: antioxidants ■ free radicals ■ heart failure ■ myocardial infarction ■ remodeling

Experimental and clinical studies have demonstrated excessive generation of reactive oxygen species (ROS) in failing hearts.[1,2] Among the potential sources of ROS within the heart, mitochondrial electron transport produces superoxide anion ($\cdot O_2^-$) in this disease state.[3] Furthermore, increased ROS leads to mitochondrial DNA (mtDNA) damage and dysfunction.[4,5] Therefore, the intimate link between mitochondrial oxidative stress, mtDNA decline, and mitochondrial dysfunction plays an important role in the development and progression of left ventricular (LV) remodeling and failure that occur after myocardial infarction (MI).

Clinical Perspective p 1786

Peroxiredoxin-3 (Prx-3) is a mitochondrial antioxidant protein and member of the Prx family that can scavenge H_2O_2 in cooperation with thiol and peroxynitrite.[6] In mammals, 6 distinct Prx family members have been identified (Prx-1 through -6). Among the Prxs, Prx-3 is unique because it is localized specifically within the mitochondria.[7] Furthermore, in vivo transfer of the *Prx-3* gene protected neurons against cell death induced by oxidative stress.[8] These beneficial characteristics make Prx-3 an important candidate for therapy against LV failure after MI, in which ROS production has been demonstrated to be increased within the mitochondria.[1,4] Although several previous reports showed the beneficial effects of antioxidants on heart failure,[9,10] no study has ever been performed to specifically examine the protective role of Prx-3. To address these questions, we created transgenic (TG) mice containing the rat *Prx-3* gene. Rat Prx-3–TG mice and their wild-type (WT) littermates were randomized to receive

Received August 10, 2005; revision received January 26, 2006; accepted February 2, 2006.

From the Department of Cardiovascular Medicine, Graduate School of Medical Sciences (S.M., T.I., H.M., M.I., T.K., K.S.), and the Department of Redox Medicinal Science, Graduate School of Pharmaceutical Sciences (M.Y.), Kyushu University, Fukuoka; Biomedical Research Laboratories (F.H., Y.H., T.K., S.O.), Daiichi Suntory Pharma Co, Ltd, Osaka; and the Department of Cardiovascular Medicine (S.K., H.T.), Hokkaido University Graduate School of Medicine, Sapporo, Japan.

Correspondence to Hiroyuki Tsutsui, MD, PhD, Department of Cardiovascular Medicine, Hokkaido University Graduate School of Medicine, Kita-15, Nishi-7, Kita-ku, Sapporo 060-8638, Japan. E-mail htsutsui@med.hokudai.ac.jp

© 2006 American Heart Association, Inc.

Circulation is available at http://www.circulationaha.org

DOI: 10.1161/CIRCULATIONAHA.105.582239

Downloaded from circ.ahajournals.org at KYUSHU UNIVERSITY on April 6, 2007

either a large transmural MI induced by coronary artery ligation or sham operation.

Methods

Generation of TG Mice

The rat Prx-3 cDNA fragment including the entire open reading frame from nucleotide 5 to 802 was amplified by polymerase chain reaction (PCR) and cloned into pCRII (Invitrogen, Carlsbad, Calif). An expression vector for Prx-3 was constructed with pQBI25 (TaKaRa), and the gene for green fluorescent protein was removed at the site of *Nhe*I-*Bam*HI. A cytomegalovirus promoter–driven expression cassette containing rat Prx-3 cDNA in the sense orientation was purified by ultracentrifugation with CsCl. The pronuclei of fertilized eggs from hyperovulated C57BL/6J mice were randomly microinjected with this DNA construct. Tail clips and a PCR protocol to confirm the genotype were performed by one group of investigators. Homozygous TG mice and C57BL/6J WT mice were used at 12 to 16 weeks of age. The study was approved by our institutional animal research committee and conformed to the animal care guidelines of the American Physiological Society.

Creation of MI

We created MI in 12- to 16-week-old, male TG mice (TG+MI) and nontransgenic WT littermates (WT+MI) by ligating the left coronary artery. Sham operation without coronary artery ligation was also performed in WT (WT+sham) and TG (TG+sham) mice. This assignment procedure was performed with the use of numeric codes to identify the animals.

Prx-3 Protein

Prx-3 protein levels were analyzed in cardiac tissue homogenates by Western blot analysis with a monoclonal antibody against rat Prx-3. Our preliminary studies revealed that this antibody against rat Prx-3 cross-reacted with mouse Prx-3 as a single band of 25 kDa. In brief, the LV tissues were homogenized with lysis buffer (20 mmol/L Tris-HCl, 1 mmol/L EDTA, 1 mmol/L EGTA, and 1 mmol/L phenylmethylsulfonylfluoride; pH 7.4). After centrifugation, equal amounts of protein (5 μg protein/lane), estimated by the Bradford method with a protein assay (Bio-Rad, Hercules, Calif), were electrophoresed on a 15% sodium dodecyl sulfate–polyacrylamide gel and then electrophoretically transferred to a nitrocellulose membrane (Millipore, Billerica, Mass). After being blocked with 5% nonfat milk in phosphate-buffered saline (PBS) containing 0.05% Tween 20 at 4°C for 1 hour, the membrane was incubated with the first antibody and then with the peroxidase-linked second antibody (Amersham Pharmacia, Uppsala, Sweden). Chemiluminescence was detected with an enhanced chemiluminescence Western blot detection kit (Amersham Pharmacia) according to the manufacturer's recommendation.

To further assess the subcellular localization of Prx-3 protein, mitochondrial and cytoplasmic fractions were prepared from LVs and subjected to Western blot analysis. In brief, the LV tissues were homogenized at 4°C for 1 minute in 6 volumes of buffer consisting of 10 mmol/L HEPES-NaOH (pH 7.4), 1 mmol/L disodium EDTA, and 250 mmol/L sucrose. The homogenate was centrifuged at 4°C and 3000*g* for 10 minutes to remove any nuclear and myofibrillar debris, and the resultant supernatant was centrifuged at 10 000*g* for 10 minutes to separate any cardiac subcellular fractions. The supernatant was used for the cytoplasmic fraction assay. To isolate the mitochondrial fraction, the pellet was resuspended at 4°C in a buffer consisting of 10 mmol/L HEPES-NaOH (pH 7.4), 1 mmol/L sodium EDTA, and 250 mmol/L sucrose and was washed 3 times with the same buffer. Murine antibodies directed toward glyceraldehyde 3-phosphate dehydrogenase (GAPDH) and cytochrome oxidase (COX) subunit I were also used to verify the integrity of these subcellular fractions.

Immunohistochemistry

Frozen sections of cardiac tissues were incubated in the presence of 100 nmol/L MitoTracker Red CMXRos (Molecular Probes, Eugene, Ore) at 37°C for 20 minutes. We did not repeat the freeze/thaw procedure to avoid the loss of mitochondrial integrity. After being washed with PBS (10 mmol/L sodium phosphate, pH 7.4, and 150 mmol/L NaCl), the sections were fixed with 3.7% formaldehyde for 5 minutes. After being washed, the fixed sections were incubated with 100-fold–diluted anti-rat Prx-3 antibody (10 μg/mL) in PBS at 4°C overnight. Fluorescence images were taken with a confocal laser scanning microscope (Bio-Rad MRC 1024) with laser beams of 488 and 568 nm for excitation.

Myocardial Antioxidant Enzyme Activities and Lipid Peroxidation

For the subsequent biochemical studies, the myocardial tissues with MI were carefully dissected into 3 parts: one consisting of the infarcted LV, one consisting of the border zone LV with the peri-infarct rim (a 1-mm rim of normal-appearing tissue), and one consisting of the remaining noninfarcted (remote) LV. The antioxidant enzymatic activities of superoxide dismutase (SOD), catalase, and glutathione peroxidase (GSHPx) were measured in the noninfarcted LV.[11] The formation of lipid peroxides was measured in the mitochondrial fraction isolated from the LV myocardium with use of a biochemical assay with thiobarbituric acid–reactive substances (TBARS).[4]

Survival

A survival analysis was performed in WT+sham (n=15), TG+sham (n=14), WT+MI (n=39), and TG+MI (n=37) mice. During the study period of 4 weeks, the cages were inspected daily for deceased animals. All deceased mice were examined for the presence of MI as well as pleural effusion and cardiac rupture.

Echocardiographic and Hemodynamic Measurements

At 4 weeks after surgery, echocardiographic studies were performed under light anesthesia with tribromoethanol/amylene hydrate (2.5% wt/vol, 8 μL/g IP) and spontaneous respiration. Two-dimensional, targeted M-mode tracings were recorded at a paper speed of 50 mm/s. Under the same anesthesia with Avertin, a 1.4F micromanometer-tipped catheter (Millar Instruments, Houston, Tex) was inserted into the right carotid artery and then advanced into the LV to measure LV pressures. One subset of investigators who were not informed of the experimental group assignments performed the in vivo LV function studies.

Infarct Size

To measure infarct size 28 days after MI, the heart was excised and the LVs were cut from apex to base into 3 transverse sections. Five-micron sections were cut and stained with Masson's trichrome. Infarct length was measured along the endocardial and epicardial surfaces in each of the cardiac sections, and the values from all specimens were summed. Infarct size (as a percentage) was calculated as total infarct circumference divided by total cardiac circumference.[12]

In addition, to measure infarct size after 24 hours (when most animals were still alive), a separate group of animals including WT+MI (n=5) and TG+MI (n=5) mice was created by ligating the left coronary artery according to the same methods described earlier. After 24 hours of coronary artery ligation, Evans blue dye (1%) was perfused into the aorta and coronary arteries, and tissue sections were weighed and then incubated with a 1.5% triphenyltetrazolium chloride solution. The infarct area (pale), the area at risk (not blue), and the total LV area from each section were measured.[13] In our preliminary study, we confirmed excellent reliability of infarct size measurements, in which a morphometric method similar to that performed in this study was used. The intraobserver and interob-

Downloaded from circ.ahajournals.org at KYUSHU UNIVERSITY on April 6, 2007

server variabilities between 2 measurements divided by these means, expressed as a percentage, were each <5%.

Myocardial Histopathology and Apoptosis

Myocyte cross-sectional area and collagen volume fraction were determined by quantitative morphometry of tissue sections from the mid-LV. To detect apoptosis, tissue sections from the mid-LV were stained with terminal deoxynucleotidyl transferase–mediated dUTP nick end-labeling (TUNEL) staining. The number of TUNEL-positive cardiac myocyte nuclei was counted, and the data were normalized per 10^5 total nuclei identified by hematoxylin-positive staining in the same sections. The proportion of apoptotic cells was counted in the noninfarcted LV. We further examined whether apoptosis was present by the more sensitive ligation-mediated PCR fragmentation assays (Maxim Biotech, Inc, Rockville, Md).

mtDNA Copy Number

DNA was extracted from cardiac tissues, and a Southern blot analysis was performed to measure the mtDNA copy number, as described earlier.[4] Primers for the mtDNA probe corresponded to nucleotides 2424 to 3605 of the mouse mitochondrial genome, and those for the nuclear-encoded mouse 18S rRNA probe corresponded to nucleotides 435 to 1951 of the human 18S rRNA genome. The mtDNA levels were normalized to the abundance of the 18S rRNA gene run on the same gel.

Mitochondrial Complex Enzyme Activity

The specific activity of mitochondrial electron transport chain complex I (rotenone-sensitive NADH-ubiquinone oxidoreductase), complex II (succinate-ubiquinone oxidoreductase), complex III (ubiquinol–cytochrome *c* oxidoreductase), and complex IV (cytochrome *c* oxidase) was measured in myocardial tissues according to methods described previously.[4] All enzymatic activities were expressed as nanomoles per minute per milligram protein.

Plasma TBARS

The formation of TBARS in peripheral blood samples from WT+MI and TG+MI mice was measured by a fluorometric assay, as described previously.[14] In brief, 100 μL of whole blood was mixed with 1 mL of saline and centrifuged at 3000*g* for 15 minutes. The supernatant was mixed with $\frac{1}{12}$N H_2SO_4 and 10% phosphotungstic acid, and the mixture was centrifuged. The sediment was suspended in distilled water, 0.3% thiobarbituric acid, and 0.1% butylated hydroxytoluene. The reaction mixture was then heated at 100°C for 60 minutes in an oil bath. After being cooled with tap water, the mixture was extracted with *n*-butanol and centrifuged at 1600*g* for 15 minutes. The fluorescence intensity of the organic phase was measured by spectrofluorometry with a wavelength of 510-nm excitation and 550-nm emission. Malondialdehyde standards (Sigma-Aldrich, St. Louis, Mo) were included with each assay batch, and plasma TBARS were expressed as micromoles per gram of plasma protein in reference to these standards.

Statistical Analysis

Data are expressed as mean±SEM. Survival analysis was performed by the Kaplan-Meier method, and between-group differences in survival were tested by the log-rank test. A between-group comparison of means was performed by 1-way ANOVA, followed by *t* tests. The Bonferroni correction was applied for multiple comparisons of means. $P<0.05$ was considered statistically significant.

The authors had full access to the data and take full responsibility for their integrity. All authors have read and agreed to the manuscript as written.

Results

We investigated 4 groups of mice, WT+sham (n=15), TG+sham (n=14), WT+MI (n=39), and TG+MI (n=37), in the present study. A survival analysis was performed for all of these mice. Subsequent echocardiographic and hemodynamic measurements were performed in the 4-week survivors: 15 WT+sham, 14 TG+sham, 25 WT+MI, and 31 TG+MI mice. These measurements could not be accomplished in 4 WT+MI and 5 TG+MI mice owing to technical difficulties. Survivor mice were further divided into 2 groups: those studied for subsequent histological analysis, including infarct size, myocyte size, and collagen volume fraction measurements as well as TUNEL staining (5 WT+sham, 5 TG+sham, 8 WT+MI, and 8 TG+MI), and those for the biochemical assay, including antioxidant enzyme activity, Prx-3 protein levels, mitochondrial lipid peroxidation, mtDNA copy number, and mitochondrial complex enzyme activities (8 WT+sham, 8 TG+sham, 8 WT+MI, and 8 TG+MI). Infarct size was not measured in the mice that died.

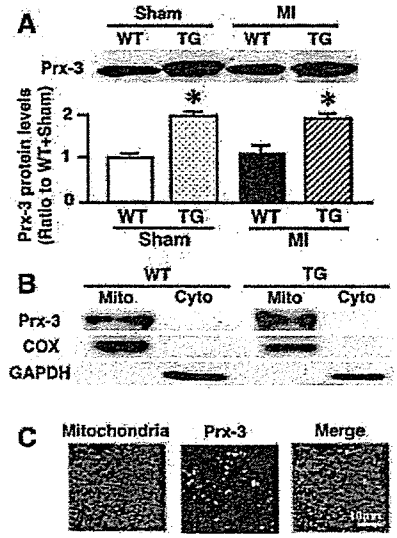

Figure 1. A, Representative Western blot analysis of Prx-3 protein levels (upper panels) and summary data (lower panels) in hearts from WT+sham, TG+sham, WT+MI, and TG+MI mice (n=6 each). Total protein extracts from the hearts were probed with a monoclonal antibody against rat Prx-3. The antibody recognized both rat and mouse Prx-3 as a single band of 25k Da. Data were obtained by densitometric quantification of the Western blots. Values are expressed as the ratio to the WT+sham value and mean±SEM. *$P<0.05$ for the difference from the ratio to WT+sham values. B, Localization of Prx-3 to mitochondria (mito). Western blot analysis of mitochondrial and cytoplasmic (cyto) fractions that were probed with antibodies directed toward Prx-3 as well as specific mitochondrial and cytoplasmic markers: GAPDH was detected in the cytoplasmic but not the mitochondrial fraction, and COX subunit I was detected in the mitochondrial but not the cytoplasmic fraction. Importantly, Prx-3 proteins were detected only in the mitochondrial fraction but not in the cytoplasmic fraction. C, Myocardial tissue sections from TG mice were doubly stained with MitoTracker dye (red) and a rat Prx-3–specific antibody (green). Immunoreactivity for Prx-3 was observed in the cytoplasm of cardiac myocytes. The merged images show that Prx-3 colocalized with the mitochondria (yellow). Scale bar=10 μm.

Myocardial Antioxidants and TBARS

First, baseline differences in Prx-3 proteins as well as other antioxidant enzyme activities between WT and TG mice were determined. In TG+sham, there was a significant increase in Prx-3 protein levels in the LV compared with that of WT+sham (Figure 1A). Importantly, the antioxidants, in-

Downloaded from circ.ahajournals.org at KYUSHU UNIVERSITY on April 6, 2007

TABLE 1. Characteristics of Animal Models

	WT+Sham	TG+Sham	WT+MI	TG+MI
Antioxidant enzymes				
n	7	7	7	7
SOD, U/mg protein	26.4±1.1	27.8±1.4	25.1±1.7	23.9±1.2
GSHPx, nmol/min per mg protein	74.1±3.2	77.7±6.7	87.8±4.8	86.1±4.2
Catalase, nmol/mg protein	79.9±6.4	85.0±6.2	87.1±3.5	81.4±5.8
Echocardiographic data				
n	15	14	21	26
Heart rate, bpm	481±11	451±8	463±13	458±8
LVEDD, mm	3.47±0.05	3.37±0.08	5.51±0.13†	4.9±0.10†§
LVESD, mm	2.22±0.05	2.12±0.10	4.78±0.13†	4.08±0.10†§
Fractional shortening, %	35.3±0.8	37.0±1.1	13.1±0.6†	16.9±0.6†§
Hemodynamic data				
n	15	14	21	26
Heart rate, bpm	447±14	455±14	453±9	466±7
Mean aortic pressure, mm Hg	83±3	78±2	76±2	77±3
LVEDP, mm Hg	2.7±0.5	2.5±0.3	11.4±1.5†	7.6±1.0*‡
Organ weight data				
n	15	14	21	26
Body wt, g	26.9±0.5	27.0±0.8	27.0±0.3	26.4±0.4
LV wt/body wt, mg/g	3.2±0.1	3.0±0.1	4.6±0.3†	4.4±0.1†
Lung wt/body wt, mg/g	5.0±0.1	5.2±0.1	7.6±0.5†	6.4±0.3†‡
Pleural effusion, %	0	0	43	15‡

EDD indicates end-diastolic diameter; ESD, end-systolic diameter; and wt, weight. Values are mean±SEM.

*P<0.05, †P<0.01 vs WT+Sham. ‡P<0.05, §P<0.01 vs WT+MI.

cluding SOD, GSHPx, and catalase activities, were not altered in the TG hearts (Table 1), indicating no effects of Prx-3 overexpression on other antioxidant enzymes. Second, the changes in antioxidants after MI were assessed. Prx-3 protein levels were significantly higher in TG+MI than in WT+MI (Figure 1A) mice. The activities of other antioxidant enzymes were not altered in WT+MI or TG+MI compared with WT+sham animals (Table 1).

The cytoplasmic marker GAPDH was detected exclusively in the cytoplasmic but not in the mitochondrial fraction, whereas COX subunit I was detected preferentially in the mitochondrial but not in the cytoplasmic fraction. This substantiates the integrity of our cellular fractions. Importantly, Prx-3 was detected only in the mitochondrial fraction but not in the cytoplasmic fraction, further confirming that Prx-3 was localized exclusively in the mitochondria (Figure 1B). In addition, immunohistochemical studies showed a homogeneous Prx-3 distribution in cardiac myocytes that colocalized with the mouse mitochondria (Figure 1C). Prx-3 staining showed a relatively spotty pattern. These results further confirm that the rat Prx-3 transgene is not expressed in the cytoplasm within the mouse heart. Mitochondrial TBARS measured in the noninfarcted LV were significantly greater in WT+MI compared with sham animals and were significantly lower in the TG+MI group (Figure 2).

Survival

There were no deaths in the sham-operated groups. Early operative mortality (within 6 hours) was comparable between WT+MI and TG+MI animals (15% versus 7%; P=NS). The survival rate up to 4 weeks tended to be higher in TG+MI compared with WT+MI mice, but this difference did not reach statistical significance (P=0.06 by log-rank test; Figure 3A). Death was suspected to be attributable to heart failure and/or arrhythmia. Five WT+MI (15%) and 2 TG+MI (5%) mice died of LV rupture (P=NS).

Infarct Size

Infarct size as determined by morphometric analysis 28 days after MI was comparable (55±1% versus 56±1%; P=0.83) between WT+MI (n=6) and TG+MI (n=6) groups. To further confirm that overexpression of Prx-3 did not alter infarct size, both the area at risk and infarct area were

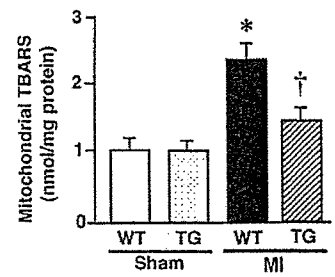

Figure 2. Mitochondrial TBARS in 4 experimental groups of animals (n=8 each). Values are mean±SEM. *P<0.05 for difference from the WT+sham value. †P<0.05 for difference from the WT+MI value.

Downloaded from circ.ahajournals.org at KYUSHU UNIVERSITY on April 6, 2007

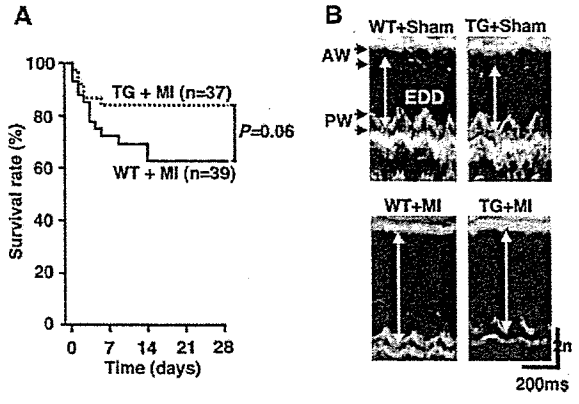

Figure 3. A, Kaplan-Meier survival analysis. Percentages of surviving WT+MI (n=39) and TG+MI (n=37) mice were plotted. Between-group difference was tested by the log-rank test. B, M-mode echocardiograms obtained from WT+sham, TG+sham, WT+MI, and TG+MI mice. AW indicates anterior wall; PW, posterior wall; and EDD, end-diastolic diameter.

measured in mice 24 hours after coronary artery ligation. Percentages of the LV at risk (risk area/LV, 51±3% versus 52±2%; $P=0.89$) and infarct size (infarct/risk area, 79±1% versus 78±1%; $P=0.13$) were also comparable between WT+MI (n=5) and TG+MI (n=5) animals.

Echocardiography and Hemodynamics

The echocardiographic and hemodynamic data of surviving mice at 28 days are shown in Figure 3B and Table 1. LV diameters were significantly larger in WT+MI mice with respect to WT+sham animals. TG+MI mice displayed less LV cavity dilatation and greater fractional shortening than did WT+MI mice. There was no significant difference in heart rate or aortic blood pressure among the 4 groups of mice. LV end-diastolic pressure (LVEDP) was higher in WT+MI than in WT+sham animals, but this increase was significantly attenuated in TG+MI mice.

Organ Weights and Histomorphometry

Coincident with an increased LVEDP, lung weight/body weight was larger in WT+MI mice, and this increase was attenuated in TG+MI mice (Table 1). The prevalence of pleural effusion was also lower in TG+MI than in WT+MI groups. Histomorphometric analysis of noninfarcted LV sections showed that myocyte cross-sectional area was greater in WT+MI mice but was significantly attenuated in TG+MI mice (Figure 4). Collagen volume fraction was greater in WT+MI mice, but this change was inhibited in TG+MI mice (Figure 4).

Myocardial Apoptosis

There were rare TUNEL-positive nuclei in sham-operated mice. The number of TUNEL-positive myocytes in the noninfarcted LV was larger in WT+MI mice but was significantly smaller in TG+MI animals (Figure 5A). In addition, the intensity of the DNA ladder indicated that apoptosis in TG+MI animals was decreased compared with that in WT+MI mice (Figure 5B).

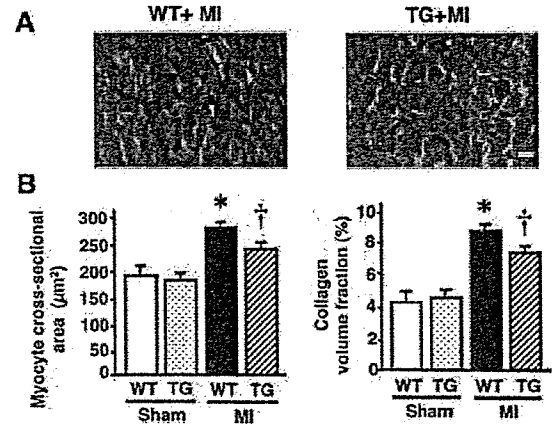

Figure 4. A, Photomicrographs of Masson trichrome–stained LV cross sections obtained from WT+MI and TG+MI mice. Scale bar=10 μm. B, Myocyte cross-sectional area and collagen volume fraction in WT+sham (n=5), TG+sham (n=5), WT+MI (n=8), and TG+MI (n=8) mice. Values are mean±SEM. *$P<0.05$ for difference from the WT+sham value. †$P<0.05$ for difference from the WT+MI value.

mtDNA and Mitochondrial Complex Enzymes Activity

Consistent with our previous studies,[4] mtDNA copy number in the noninfarcted LV from WT+MI animals showed a 36% decrease ($P<0.05$) compared with that in sham-operated mice, which was significantly prevented and was preserved at normal levels in TG+MI animals (Figure 6).

To determine the effects of mtDNA alterations on mitochondrial function, we next measured the mitochondrial electron transport chain complex enzyme activities. The enzymatic activities of complexes I, III, and IV were significantly lower in the noninfarcted LV from WT+MI than in those from WT+sham animals (Table 2). Most important, no such decrease was observed in TG+MI mice. The enzymatic activity of complex II, exclusively encoded by nuclear DNA, was not altered in either group. These results indicate that mtDNA copy number and mitochondrial complex enzymatic activities are downregulated in the post-MI heart and that Prx-3 gene overexpression efficiently counteracts these mitochondrial deficiencies.

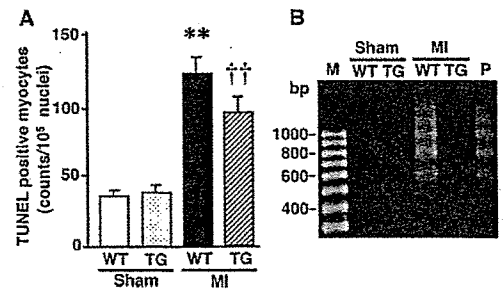

Figure 5. A, Numbers of TUNEL-positive myocytes in the noninfarcted LV from WT+sham, TG+sham, WT+MI, and TG+MI mice (n=5 each). Values are mean±SEM. **$P<0.01$ for the difference from the WT+sham value. ††$P<0.01$ for the difference from the WT+MI value. B, DNA ladder indicative of apoptosis in the genomic DNA from the LV. M indicates marker; P, positive control.

Downloaded from circ.ahajournals.org at KYUSHU UNIVERSITY on April 6, 2007

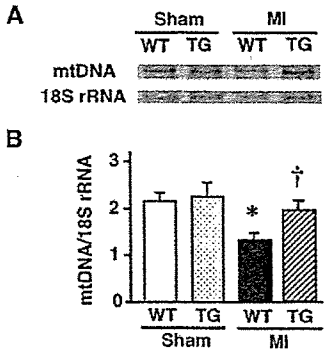

Figure 6. A, Southern blot analysis of mtDNA copy number in total DNA extracts from the hearts from WT+sham, TG+sham, WT+MI, and TG+MI mice. Top bands show signals from the mtDNA fragments, and bottom bands show signals from the nuclear DNA fragments containing the 18S rRNA gene. B, Summary data for a Southern blot analysis of mtDNA copy number in 4 groups of animals (n=8 each). Data were obtained by densitometric quantification of the Southern blots, such as shown in A. Values are expressed as the ratio to WT+sham values and mean±SEM. *$P<0.05$ for the difference from the WT+sham value. †$P<0.05$ for the difference from the WT+MI value.

Plasma TBARS

Plasma TBARS were comparable between WT+MI and TG+MI mice (0.46±0.04 versus 0.54±0.05 μmol/g protein; P=NS).

Discussion

The present study provides the first direct evidence that overexpression of mitochondrial antioxidant Prx-3 protects the heart against post-MI remodeling and failure in mice. It reduced LV cavity dilatation and dysfunction, as well as myocyte hypertrophy, interstitial fibrosis, and apoptosis of the noninfarcted myocardium. These beneficial effects of *Prx-3* gene overexpression were associated with an attenuation of mitochondrial oxidative stress, mtDNA decline, and dysfunction. They were not due to its MI size-sparing effect but occurred secondary to more adaptive remodeling.

Mitochondria are the predominant source of ROS in the failing myocardium.[1] Most of the $\cdot O_2^-$ generated by the mitochondria is vectorially released into the mitochondrial matrix. $\cdot O_2^-$ impairs mitochondrial function by oxidizing the Fe-S centers of complex enzymes. In addition, $\cdot O_2^-$ is converted to peroxynitrite, an extremely powerful oxidant, as a result of its reaction with NO produced by mitochondrial NO synthase. $\cdot O_2^-$ is also converted to H_2O_2 by a specific intramitochondrial Mn-SOD. Although Mn-SOD relieves mitochondrial oxidative stress caused by $\cdot O_2^-$, it generates H_2O_2 and therefore, further enhances a different type of oxidative stress. H_2O_2 can damage cellular macromolecules such as proteins, lipids, and nucleic acids, especially after its conversion to ·OH. Moreover, these increased ROS in the mitochondria were associated with a decreased mtDNA copy number and reduced oxidative capacity owing to low complex enzyme activities.[4] Therefore, chronic increases in mitochondrial ROS production cause mtDNA damage and dysfunction, which thus, can lead to a catastrophic cycle of further oxidative stress and ultimate cellular injury.[5] This deleterious process may play an important role in the development and progression of myocardial remodeling and failure.[4] Based on these results, mitochondrial antioxidants are expected to be the first line-of-defense mechanism against ROS generation in the mitochondria and ROS-mediated mitochondrial injury and thus, may protect the heart from adverse remodeling and failure.

Prx-3, which was formerly known as SP-22, or MER5, is currently identified as a mitochondrial member of the novel antioxidant proteins designated as Prxs.[15] Among 6 known mammalian Prxs, Prx-1 to -4 require the small redox protein thioredoxin (Trx) as an electron donor to remove H_2O_2, whereas Prx-5 and -6 can use other cellular reductants, such as GSH, as their electron donor.[16] Prx-1, -2, and -6 are found in the cytoplasm and nucleus,[7] whereas Prx-3 contains a mitochondrial localization sequence, is found exclusively in the mitochondria, and uses mitochondrial Trx-2 as the electron donor for its peroxidase activity.[17] It functions not only by removing H_2O_2 formed after the SOD-catalyzed dismutation reaction but also by detoxifying peroxynitrite.[6] Therefore, the great efficiency of Prx-3 as an antioxidant shown in the present study may be attributable to the fact that it is located in the mitochondria and can utilize lipid peroxides as well as H_2O_2 for substrates. In fact, overexpression of Prx-3 has been shown to protect thymoma cells from apoptosis induced by hypoxia, a bolus of peroxide, or an anticancer drug.[18] Moreover, Prx-3 overexpression has been reported to protect rat hippocampal neurons from excitotoxic injury.[8] Prx-5 is also associated with the mitochondria in addition to the peroxisomes and nucleus. Recently, increased expression of Prx-5 was found to have protected Chinese hamster ovary cells from mtDNA damage induced by oxidative stress.[19] Therefore, Prx-5 may also exert beneficial effects against mitochondrial oxidative stress in post-MI hearts.

GSHPx also catalyzes the reduction of H_2O_2. In fact, our previous studies demonstrated that overexpression of GSHPx

TABLE 2. Mitochondrial Complex Enzyme Activities

	WT+Sham	TG+Sham	WT+MI	TG+MI
n	7	7	7	7
Complex I, nmol/min per mg protein	282±26	265±38	159±25*	287±16†
Complex II, nmol/min per mg protein	770±70	718±93	711±85	726±128
Complex III, nmol/min per mg protein	505±11	470±31	367±20*	451±21†
Complex IV, nmol/min per mg protein	1223±37	1175±34	744±68*	939±54†

Values are mean±SEM.
*$P<0.05$ vs WT+sham; †$P<0.05$ vs WT+MI.

Downloaded from circ.ahajournals.org at KYUSHU UNIVERSITY on April 6, 2007

inhibited LV remodeling and failure after MI.[13] However, GSHPx is located predominantly in the cytosol, and only a small proportion (≈10%) is present in the mitochondria.[20] Therefore, it remains unclear whether the beneficial effects of GSHPx overexpression on post-MI hearts were attributable to an increase of this enzyme in the cytosol, the mitochondria, or both. The specific localization of Prx-3 in the mitochondria suggests that mitochondrial oxidative stress plays an important role in the development and progression of heart failure, and antioxidants localized specifically within the mitochondria provide a primary line of defense against this disease process.

A growing body of evidence suggests that ROS play a major role in the pathogenesis of cardiac failure. Furthermore, antioxidants have been shown to exert protective and beneficial effects against heart failure.[21,22] A previous study from our laboratory demonstrated that dimethylthiourea improved survival and prevented LV remodeling and failure after MI.[10] However, the most effective way to evaluate the contribution of any specific antioxidant and obtain direct evidence of an adverse role for ROS in heart failure is through gene manipulation. Therefore, the present study not only extends the previous observation that used antioxidants but also reveals the major role of mitochondrial oxidative stress in the pathophysiology of post-MI remodeling and failure.

The beneficial effects of Prx-3 overexpression shown in the present study were not due to its MI size-sparing effect, because there was no statistically significant difference in infarct size between WT+MI and TG+MI mice. Furthermore, its effects were not attributable to hemodynamics because blood pressures and heart rates were not altered (Table 1). Importantly, it is also unlikely that these effects were caused by the altered expression of antioxidant enzymes other than Prx-3 (Table 1). Moreover, the beneficial effects of Prx-3 overexpression were not due to systemic induction of antioxidant defenses. This possibility is less likely because plasma TBARS were comparable between WT+MI and TG+MI mice. Nevertheless, we cannot completely exclude the possibility that the systemic effects of Prx-3 induction might also have contributed to this phenotype because this TG is not heart-specific.

There may be several factors contributing to the protective effects conferred by Prx-3 overexpression on post-MI remodeling and failure. First, recent studies have demonstrated that a Trx-related antioxidant system is closely associated with the regulation of apoptosis, probably through quenching of ROS and redox control of the mitochondrial permeability transition pores that release cytochrome *c*.[23] A subtle increase in ROS caused by partial inhibition of SOD results in apoptosis in isolated cardiac myocytes.[24] Previous studies have demonstrated that apoptosis appears not only in infarcted but also in noninfarcted myocardium after MI.[25] Specifically, apoptosis occurs in the noninfarcted LV late after MI. This is an intriguing observation, in light of the remodeling process known to occur within the noninfarcted area, which is characterized by the loss of myocytes and hypertrophy. In fact, recent studies have suggested cardiac myocyte apoptosis contributes to LV remodeling after MI.[26,27] Importantly, increased oxidative stress occurs concomitantly with increased cardiac myocyte apoptosis within the noninfarcted area. This is a provoking observation, because oxidative stress is a powerful inducer of apoptotic cell death.[28] The present study suggests that the coexistence of oxidative stress and myocyte apoptosis in the noninfarcted LV after MI is causally related. Oxidative stress may mediate myocyte apoptosis, which may lead to myocardial remodeling and failure. Therefore, the decreased mitochondrial oxidative stress due to Prx-3 overexpression could contribute to the amelioration of apoptosis (Figure 5) and eventual post-MI cardiac failure. Second, Prx-3 overexpression prevented the decrease in mtDNA copy number (Figure 6) as well as mitochondrial complex enzyme activities (Table 2). Our previous studies have demonstrated an intimate link between mtDNA damage, increased lipid peroxidation, and a decrease in mitochondrial function, which might play a major role in the development and progression of cardiac failure.[4]

There are several issues to be acknowledged as limitations of this study. First, the differences between WT+MI and TG+MI groups in their echocardiographic measurements are not remarkable, even though they are statistically significant (Table 1). However, our previous study showed that the intraobserver and interobserver variabilities in our echocardiographic measurements for LV dimensions were small, and measurements made in the same animals on separate days were highly reproducible.[12] Therefore, these values are considered to be valid. Second, longer-term follow-up data are not available for the animals in the current study. We therefore could not determine whether the differences between WT+MI and TG+MI groups seen in the present study were more or less significant at later time points, when additional LV remodeling would have been expected to occur.

In conclusion, Prx-3 overexpression inhibited the development of LV remodeling and failure after MI, which was associated with an attenuation of myocyte hypertrophy, apoptosis, and interstitial fibrosis. It also ameliorated mitochondrial oxidative stress as well as mtDNA decline and mitochondrial dysfunction in post-MI hearts. Therapies designed to interfere with mitochondrial oxidative stress could be beneficial to prevent heart failure after MI.

Acknowledgments

This study was supported in part by grants from the Ministry of Education, Science and Culture (No. 12670676, 14370230, 17390223). A portion of this study was conducted at Kyushu University Station for Collaborative Research I and II.

Disclosures

None.

References

1. Ide T, Tsutsui H, Kinugawa S, Suematsu N, Hayashidani S, Ichikawa K, Utsumi H, Machida Y, Egashira K, Takeshita A. Direct evidence for increased hydroxyl radicals originating from superoxide in the failing myocardium. *Circ Res*. 2000;86:152–157.
2. Mallat Z, Philip I, Lebret M, Chatel D, Maclouf J, Tedgui A. Elevated levels of 8-iso-prostaglandin F2α in pericardial fluid of patients with heart failure: a potential role for in vivo oxidant stress in ventricular dilatation and progression to heart failure. *Circulation*. 1998;97:1536–1539.

Downloaded from circ.ahajournals.org at KYUSHU UNIVERSITY on April 6, 2007

3. Ide T, Tsutsui H, Kinugawa S, Utsumi H, Kang D, Hattori N, Uchida K, Arimura K, Egashira K, Takeshita A. Mitochondrial electron transport complex I is a potential source of oxygen free radicals in the failing myocardium. *Circ Res.* 1999;85:357–363.
4. Ide T, Tsutsui H, Hayashidani S, Kang D, Suematsu N, Nakamura K, Utsumi H, Hamasaki N, Takeshita A. Mitochondrial DNA damage and dysfunction associated with oxidative stress in failing hearts after myocardial infarction. *Circ Res.* 2001;88:529–535.
5. Suematsu N, Tsutsui H, Wen J, Kang D, Ikeuchi M, Ide T, Hayashidani S, Shiomi T, Kubota T, Hamasaki N, Takeshita A. Oxidative stress mediates tumor necrosis factor-α–induced mitochondrial DNA damage and dysfunction in cardiac myocytes. *Circulation.* 2003;107:1418–1423.
6. Bryk R, Griffin P, Nathan C. Peroxynitrite reductase activity of bacterial peroxiredoxins. *Nature.* 2000;407:211–215.
7. Kang SW, Chae HZ, Seo MS, Kim K, Baines IC, Rhee SG. Mammalian peroxiredoxin isoforms can reduce hydrogen peroxide generated in response to growth factors and tumor necrosis factor-α. *J Biol Chem.* 1998;273:6297–6302.
8. Hattori F, Murayama N, Noshita T, Oikawa S. Mitochondrial peroxiredoxin-3 protects hippocampal neurons from excitotoxic injury in vivo. *J Neurochem.* 2003;86:860–868.
9. Sia YT, Lapointe N, Parker TG, Tsoporis JN, Deschepper CF, Calderone A, Pourdjabbar A, Jasmin JF, Sarrazin JF, Liu P, Adam A, Butany J, Rouleau JL. Beneficial effects of long-term use of the antioxidant probucol in heart failure in the rat. *Circulation.* 2002;105:2549–2555.
10. Kinugawa S, Tsutsui H, Hayashidani S, Ide T, Suematsu N, Satoh S, Utsumi H, Takeshita A. Treatment with dimethylthiourea prevents left ventricular remodeling and failure after experimental myocardial infarction in mice: role of oxidative stress. *Circ Res.* 2000;87:392–398.
11. Ho YS, Magnenat JL, Bronson RT, Cao J, Gargano M, Sugawara M, Funk CD. Mice deficient in cellular glutathione peroxidase develop normally and show no increased sensitivity to hyperoxia. *J Biol Chem.* 1997;272:16644–16651.
12. Shiomi T, Tsutsui H, Hayashidani S, Suematsu N, Ikeuchi M, Wen J, Ishibashi M, Kubota T, Egashira K, Takeshita A. Pioglitazone, a peroxisome proliferator–activated receptor-γ agonist, attenuates left ventricular remodeling and failure after experimental myocardial infarction. *Circulation.* 2002;106:3126–3132.
13. Shiomi T, Tsutsui H, Matsusaka H, Murakami K, Hayashidani S, Ikeuchi M, Wen J, Kubota T, Utsumi H, Takeshita A. Overexpression of glutathione peroxidase prevents left ventricular remodeling and failure after myocardial infarction in mice. *Circulation.* 2004;109:544–549.
14. Ide T, Tsutsui H, Ohashi N, Hayashidani S, Suematsu N, Tsuchihashi M, Tamai H, Takeshita A. Greater oxidative stress in healthy young men compared with premenopausal women. *Arterioscler Thromb Vasc Biol.* 2002;22:438–442.
15. Wood ZA, Schroder E, Robin Harris J, Poole LB. Structure, mechanism and regulation of peroxiredoxins. *Trends Biochem Sci.* 2003;28:32–40.
16. Fisher AB, Dodia C, Manevich Y, Chen JW, Feinstein SI. Phospholipid hydroperoxides are substrates for non-selenium glutathione peroxidase. *J Biol Chem.* 1999;274:21326–21334.
17. Watabe S, Hiroi T, Yamamoto Y, Fujioka Y, Hasegawa H, Yago N, Takahashi SY. SP-22 is a thioredoxin-dependent peroxide reductase in mitochondria. *Eur J Biochem.* 1997;249:52–60.
18. Nonn L, Berggren M, Powis G. Increased expression of mitochondrial peroxiredoxin-3 (thioredoxin peroxidase-2) protects cancer cells against hypoxia and drug-induced hydrogen peroxide–dependent apoptosis. *Mol Cancer Res.* 2003;1:682–689.
19. Banmeyer I, Marchand C, Clippe A, Knoops B. Human mitochondrial peroxiredoxin 5 protects from mitochondrial DNA damages induced by hydrogen peroxide. *FEBS Lett.* 2005;579:2327–2333.
20. Chang TS, Cho CS, Park S, Yu S, Kang SW, Rhee SG. Peroxiredoxin III, a mitochondrion-specific peroxidase, regulates apoptotic signaling by mitochondria. *J Biol Chem.* 2004;279:41975–41984.
21. Dhalla AK, Hill MF, Singal PK. Role of oxidative stress in transition of hypertrophy to heart failure. *J Am Coll Cardiol.* 1996;28:506–514.
22. Nakamura R, Egashira K, Machida Y, Hayashidani S, Takeya M, Utsumi H, Tsutsui H, Takeshita A. Probucol attenuates left ventricular dysfunction and remodeling in tachycardia-induced heart failure: roles of oxidative stress and inflammation. *Circulation.* 2002;106:362–367.
23. Petronilli V, Costantini P, Scorrano L, Colonna R, Passamonti S, Bernardi P. The voltage sensor of the mitochondrial permeability transition pore is tuned by the oxidation-reduction state of vicinal thiols: increase of the gating potential by oxidants and its reversal by reducing agents. *J Biol Chem.* 1994;269:16638–16642.
24. Siwik DA, Tzortzis JD, Pimental DR, Chang DL, Pagano PJ, Singh K, Sawyer DB, Colucci WS. Inhibition of copper-zinc superoxide dismutase induces cell growth, hypertrophic phenotype, and apoptosis in neonatal rat cardiac myocytes in vitro. *Circ Res.* 1999;85:147–153.
25. Palojoki E, Saraste A, Eriksson A, Pulkki K, Kallajoki M, Voipio-Pulkki LM, Tikkanen I. Cardiomyocyte apoptosis and ventricular remodeling after myocardial infarction in rats. *Am J Physiol Heart Circ Physiol.* 2001;280:H2726–H2731.
26. Sam F, Sawyer DB, Chang DL, Eberli FR, Ngoy S, Jain M, Amin J, Apstein CS, Colucci WS. Progressive left ventricular remodeling and apoptosis late after myocardial infarction in mouse heart. *Am J Physiol Heart Circ Physiol.* 2000;279:H422–H428.
27. Oskarsson HJ, Coppey L, Weiss RM, Li WG. Antioxidants attenuate myocyte apoptosis in the remote non-infarcted myocardium following large myocardial infarction. *Cardiovasc Res.* 2000;45:679–687.
28. von Harsdorf R, Li PF, Dietz R. Signaling pathways in reactive oxygen species–induced cardiomyocyte apoptosis. *Circulation.* 1999;99:2934–2941.

CLINICAL PERSPECTIVE

A growing body of evidence suggests that oxidative stress, an excess generation of reactive oxygen species (ROS), plays a major role in the pathogenesis of heart failure. Furthermore, antioxidants have been shown to exert protective and beneficial effects against this process. Recent studies have suggested that mitochondria are the predominant source of ROS in the failing heart, and mitochondrial antioxidants are expected to be the first line of defense against mitochondrial oxidative stress–mediated myocardial injury. The present study demonstrated that overexpression of peroxiredoxin-3 (Prx-3) inhibited cardiac remodeling and failure after myocardial infarction (MI) created by ligation of the left coronary artery in mice. Prx-3 contains a mitochondrial localization sequence, is found exclusively in the mitochondria, and uses mitochondrial thioredoxin (Trx)-2 as the electron donor for its peroxidase activity. It functions not only by removing H_2O_2 formed after the superoxide dismutase (SOD)–catalyzed dismutation reaction but also by detoxifying peroxynitrite. Therefore, the great efficiency of Prx-3 as an antioxidant shown in the present study may be attributable to the fact that it is located in the mitochondria and can utilize lipid peroxides as well as H_2O_2 for substrates. The present study not only extends previous investigations that used antioxidants but also reveals a major role for mitochondrial oxidative stress in the pathophysiology of postinfarct heart failure. Therapies designed to interfere with mitochondrial oxidative stress by using antioxidant Prx-3 might also beneficial in preventing clinical heart failure.

Downloaded from circ.ahajournals.org at KYUSHU UNIVERSITY on April 6, 2007

ELSEVIER

Journal of Neuroscience Methods 156 (2006) 71–75

JOURNAL OF NEUROSCIENCE METHODS

www.elsevier.com/locate/jneumeth

Reversible vagal blockade in conscious rats using a targeted delivery device

Can Zheng [a,*], Toru Kawada [a], Meihua Li [a], Takayuki Sato [b], Kenji Sunagawa [c], Masaru Sugimachi [a]

[a] *Department of Cardiovascular Dynamics, Advanced Medical Engineering Center, National Cardiovascular Center Research Institute, 5-7-1 Fujishirodai, Suita-shi, Osaka 565-8565, Japan*

[b] *Department of Physiology, Kochi Medical School, Kochi 783-8505, Japan*

[c] *Department of Cardiovascular Medicine, Graduate School of Medical Sciences, Kyushu University, Fukuoka 812-8582, Japan*

Received 30 November 2005; received in revised form 7 February 2006; accepted 8 February 2006

Abstract

Reversible methods of nerve blockade greatly aid neurophysiological and behavioral studies. We have developed an implantable device for the local delivery of anesthetics to the area surrounding the vagal nerve in rats. The device consists of a thick silicone tube for insulating the nerves from the surrounding tissue, and a thin silicone tube for the infusion of anesthetics into the insulating tube. The in vivo performance of the device was tested electrophysiologically, and cardiovascular responses to vagal stimulation were measured in conscious animals. Nerve conductivity was completely blocked by injection of a small amount (<20 μl) of 1% lidocaine, with conductivity subsequently recovering gradually after 10–40 min. Electrical stimulation of the right vagus nerve in conscious rats increased arterial pressure while decreasing heart rate. The local blockade of afferent fibers abolished the arterial pressure response but preserved the bradycardic response to vagal nerve stimulation. The targeted delivery device was useful for reversible vagal blockade in conscious rats.

© 2006 Elsevier B.V. All rights reserved.

Keywords: Vagus; Conduction blockade; Electric stimulation; Heart rate; Blood pressure; Conscious; Rat

1. Introduction

Peripheral nerves are the first step in the pathway that conducts signals from various peripheral sensors to the central nervous system (CNS) and are also the output pathway for signals from the CNS to various organs, with most peripheral nerves containing both afferent and efferent fibers. In the investigation of the integrative functions of the autonomic nervous system, several techniques have been developed for performing nerve blockade for recording or selectively stimulating either afferent or efferent fibers. One such technique is surgical denervation, which effectively eliminates nerve conduction, but is irreversible and may not be applicable to the vagus nerve in the chronic experimental settings, as animals cannot survive for long after bilateral vagotomy. Nerve cooling provides a reversible nerve blockade in conscious large animals (Derksen et al., 1981; Borgdorff and Versteeg, 1984; Cudd, 1998) and in anesthetized small animals (Vizek et al., 1983; Schultz et al., 1988; Lee et al., 1990), but is difficult in conscious small animals such as rats, due to technical problems associated with the size of the nerve cooling device. Alternatively, local anesthetics such as lidocaine are widely used for nerve blockade in clinical practice and animal studies (Thalhammer et al., 1995; Gokin et al., 2001; Potocnik et al., 2001). The major advantages of anesthetics for nerve blockade are the complete reversibility of the nerve blockade and the ease of administration. However, it can be difficult to administer local anesthetics in small conscious animals, largely because the vagus nerve runs close to the common carotid artery and the aortic depressor nerve, and therefore the injection procedure may result in artery or nerve damage. A technique of delivering neurotrophins or anesthetics to the sciatic nerve has been demonstrated in the conscious rat model (Kanje et al., 1988; Costanzo et al., 1999). However, it is not yet known whether such a targeted delivery method can be used to block the vagus nerve in conscious rats. In this study, we designed a targeted delivery device for the rat vagus nerve, which allowed local

* Corresponding author. Tel.: +81 6 6833 5012x2427; fax: +81 6 6835 5403.
E-mail address: zhengcan@ri.ncvc.go.jp (C. Zheng).

0165-0270/$ – see front matter © 2006 Elsevier B.V. All rights reserved.
doi:10.1016/j.jneumeth.2006.02.015

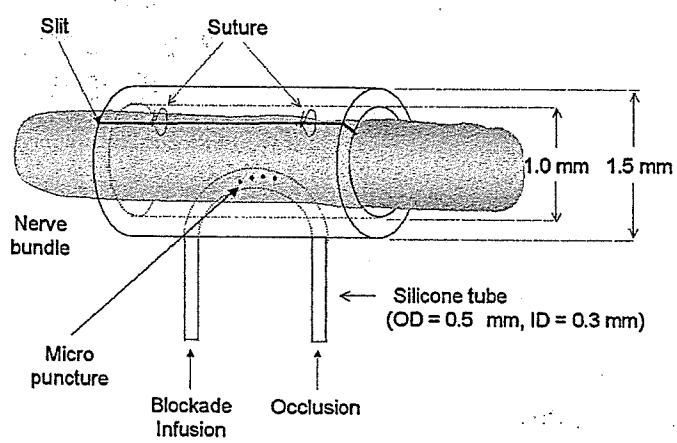

Fig. 1. Schematic illustration of the design of the targeted delivery device for the rat vagus nerve.

infusion of anesthetics into the area surrounding the nerve. The aim of this study was to evaluate this targeted delivery device for vagal blockade in conscious rats.

2. Materials and methods

2.1. A targeted delivery device

We designed an implantable device for delivering anesthetics to the area surrounding the rat cervical vagus nerve. As shown in Figs. 1 and 2E, this device was composed of a thick silicone tube (i.d. = 1.0 mm; o.d. = 1.5 mm; L = 3–4 mm) acting as a nerve guiding tube, and a thin silicone tube (i.d. = 0.3 mm; o.d. = 0.5 mm) for the injection of anesthetic agents. We made a longitudinal slit in the thick tube and pierced two holes in the wall of this tube for the thin tube to pass in and out of. Several micro-punctures were made by a microneedle (with a tip of 0.01 mm) in the inner part of the thin tube to allow the anesthetics to leak out into the guide tube.

We injected anesthetics slowly from one end of the thin tube until the liquid anesthetics replaced the air in the tube, and then we occluded the other end while increasing the pressure in the thin tube to force the liquid to leak out through the micro-punctures into the area surrounding the nerve. In the present study, we used 1% lidocaine solution for local blockade of vagal conduction. After completion of the experimental protocol, we flushed the tubes with distilled water to prevent the micro-punctures from becoming occluded by residual anesthetics.

2.2. Surgical preparation

Experiments were performed on six Sprague–Dawley rats weighing between 320 and 450 g. Animals were cared for in strict accordance with the Guiding Principles for the Care and Use of Animals in the Field of Physiological Science approved by the Physiological Society of Japan. Under 1.5%-halothane anesthesia, the lead wires of the cuff electrodes and the infusion tubes were tunneled subcutaneously from the back where they were fixed to a custom-designed multi-channel skin connector (Fig. 2B and G). The right vagus nerve was carefully dissected away from the common carotid artery and placed into the guide tube. The slit in the guide tube was then sutured by a polypropylene suture (8-0, ETHICON, INC.). Two custom-designed cuff electrodes, each having a pair of stainless steel wire electrodes (Fig. 2F), were implanted into the nerve trunk in the proximal and distal sides of the guide tube at a distance of 1.1–1.4 mm. Next, a blood pressure telemeter (TA11PA-C40, DSI) was implanted into the abdomen with a pressure sensor inserted into the abdominal aorta for monitoring mean arterial pressure (MAP) and heart rate (HR). After recovery from the surgical procedure, the animals were maintained on standard rat chow ad libitum, and were restrained in a rodent cage for physiological measurements as described below.

2.3. Experimental protocols

The experimental protocols were conducted at least 1 week after the implantation surgery. The in vivo effectiveness of the targeted delivery for nerve blockade was evaluated electrophysiologically and by measurement of HR and MAP responses to

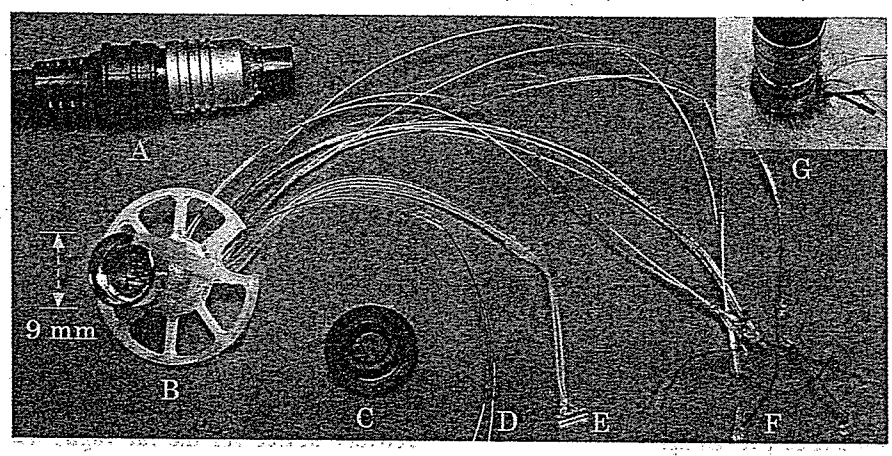

Fig. 2. Photographic images of the multi-channel skin connector with electrodes and nerve blocker. (A) Plug, (B) skin connector with 12-pin receptacle, (C) cap, (D) ECG leads, (E) nerve blocker, (F) nerve electrodes, the leads were extended with flexible coil (made of stainless wire of 0.03 mm in diameter, epoxy coated) and tips were fixed in the slit silicone tube (i.d. = 0.5; o.d. = 1 mm), and (G) implanted skin connector with local infusion setting.

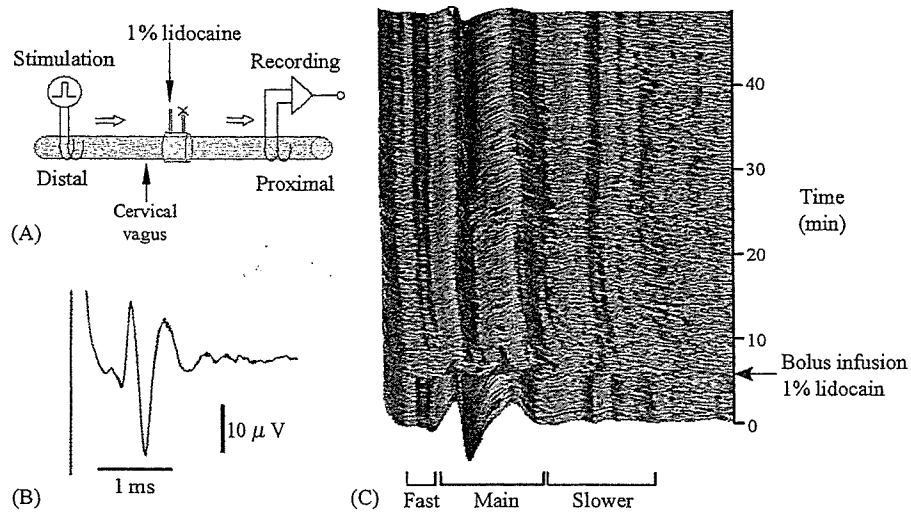

Fig. 3. Example of in vivo electrophysiology of the rat vagus. (A) A diagram of the experimental arrangement. (B) Compound action potential (CAP) of the right vagus evoked by the electrical pulse (1 Hz, 0.3 ms, 1.3 V). (C) The inhibition of vagal conduction by local injection of a small amount (<20 μl) of 1% lidocaine in conscious rats. Each trace was obtained as a result of waveform averaging of 10 single successive sweeps.

electrical stimulation of the vagus nerve in conscious animals. While the rat was loosely restrained in a rodent cage, lead wires for nerve stimulation and recording were attached to the skin connector (Fig. 2A and B). Arterial pressure was measured by telemetry. After carefully arranging the two electrodes and the delivery device, nerve stimulation with either distal or proximal nerve blockade was performed.

Nerve impulses were evoked by electrical stimulation of the vagus from the cuff electrode distal to the targeted delivery device (Fig. 3A). Rectangular pulses were delivered using a stimulator (SEN-7103, Nihon Kohden) and an isolator (SS-202J, Nihon Kohden). For in vivo electrophysiology, the stimulation frequency was 1 Hz and the pulse duration was 0.3 ms. The magnitude of stimulation was set at a supramaximal level (1.2–2.0 V). For functional experiments examining the AP and HR responses, the stimulation frequency, pulse duration, and magnitude were set at 10–30 Hz, 0.2–1 ms, and 2 V, respectively. The compound action potential (CAP) was amplified using an AC amplifier (200,000×, Model AB-610J, Nihon Kohden) with low (150 Hz) and high (1 kHz) frequency cutoffs. Nerve signals and arterial pressure data were sampled using a 12-bit A/D converter. Nerve signals were digitized at 5 kHz per electrode channel. The data were saved onto the hard disk of a dedicated laboratory computer system for later analysis.

2.4. Statistics

Data were reported as mean ± S.D. values. Changes in HR and MAP were compared before and during the stimulation by paired *t*-tests with the significance level set at $p < 0.05$.

3. Results

Fig. 3B shows the CAP of the vagus nerve evoked by electrical stimulation from the cuff electrode. The CAP consisted of one main component propagating at 0.9–2.1 m/s, as well as fast (>3 m/s) and slow (<0.9 m/s) components. All components of the CAP disappeared after an injection of a small amount (<20 μl) of 1% lidocaine (Fig. 3C). The fast component had almost recovered 15 min after the injection, followed by recovery of the main component in 40 min. The slow component required longer to recover.

The rats stayed quiet during the injection of anesthetics, with no changes in baseline HR and MAP. The HR and AP responses to electric stimulation differed after blockade of the afferent nerves, compared with before blockade. Prior to nerve blockade, electric stimulation of the right vagus nerve decreased HR abruptly, whereas it was associated with an increase in MAP, as shown in Fig. 4; HR decreased from 434 ± 8 to 246 ± 35 bpm ($p < 0.01$), whereas MAP increased from 99 ± 11 to 127 ± 14 mmHg ($p < 0.01$). However, after the blockade of afferent fibers, electrical stimulation of the nerve decreased HR without significant changes in MAP (HR 414 ± 4 bpm versus 266 ± 17 bpm, $p < 0.01$; MAP 106 ± 12 mmHg versus 103 ± 14 mmHg). The effects of vagal afferent blockade were

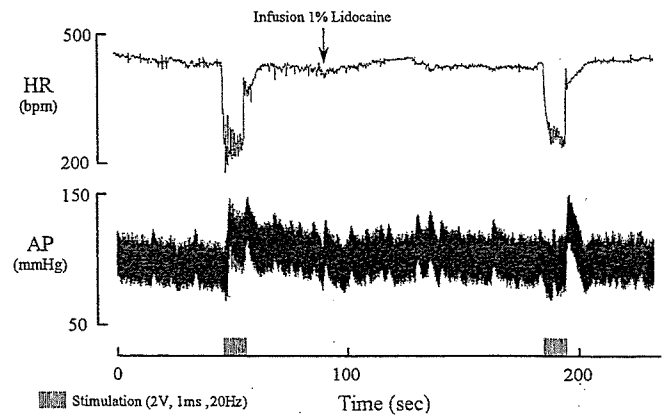

Fig. 4. Representative responses of arterial pressure (AP) and heart rate (HR) to electric stimulation (2 V, 1 ms, 20 Hz, 10 s) of the right vagus nerve before and after blockade of afferent fibers by local infusion of 1% lidocaine in conscious rats.

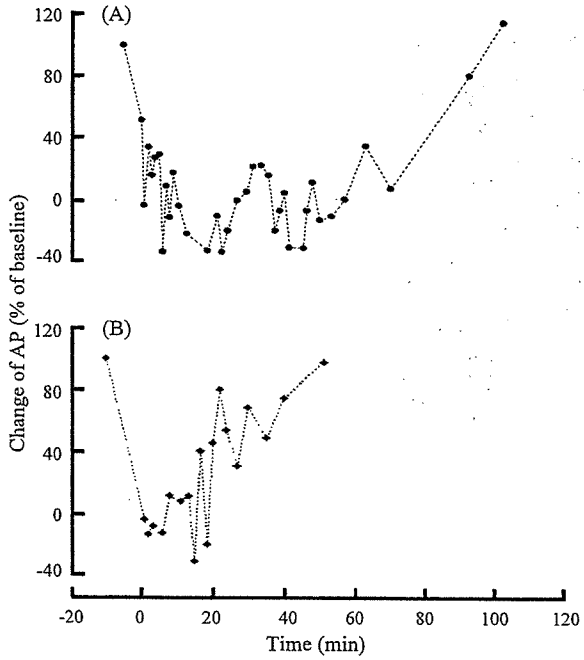

Fig. 5. Examples of the time course of the arterial pressure (AP) response to electric stimulation of cervical vagus nerve after afferent blockade by bolus infusion of 1% lidocaine in conscious rats. Each point represents the percentage of AP responses compared to the baseline response (before afferent blockade). Electric stimulations (2 V, 1 ms, 20 Hz, 10 s) were performed intermittently at interval greater than 1 min. The tests were done 1 week (A) and 2 weeks (B) after the implantation surgery.

reversible and the HR and MAP responses were restored in 15–60 min after the injection of 1% lidocaine. The duration of the nerve block was shorter in the second week than the first week (Fig. 5). The durability of the targeted delivery device was chiefly determined by how intact the infusion tube was. The effectiveness of the local blockade was confirmed 2 months after the implantation surgery.

4. Discussion

A variety of disease models, ranging from hypertension to heart failure, make the rat very important as an experimental animal for cardiovascular research. Reversible blockade of the autonomic nerves in small animals like the rat would be useful for physiological and behavioral study (Thalhammer et al., 1995), and would contribute to our understanding of the regulation of the cardiovascular system by the autonomic nervous system. We designed a targeted delivery device for the rat cervical vagus nerve. Using the targeted delivery device, in vivo electrophysiology and the functional evaluation of reversible nerve blockade were conducted in chronically instrumented, conscious rats. To our knowledge, this is the first study applying the targeted delivery device to blockade of the vagus nerve in conscious rats.

As shown in Fig. 3C, local injection of a small amount (<20 μl) of anesthetic (1% lidocaine) caused reversible, complete conduction block of the vagus nerve. The rats stayed calm in the rodent cage without any indication of significant stress during or after the injection of anesthetics. Temporary administration of anesthetics via the targeted delivery device lessens the stress compared to other techniques of nerve blockade requiring surgical procedures, and is therefore suitable for evaluating the role of the autonomic nervous system in circulatory regulation without significant sympathetic excitation associated with the stress. The infusion period and the type of anesthetics may control the duration of nerve blockade. For instance, lidocaine causes a relatively short-lived nerve blockade whereas marcaine causes a longer blockade. Selective anesthetics may also be used for vagal afferent blockade (Bowser-Riley et al., 1990). Fig. 5 shows that the duration of the nerve block lessoned over time after the implantation surgery even with the same dose of anesthetic. The space surrounding the nerve within the guide tube may be replaced by regenerated tissue over time after the surgical procedure, possibly reducing the effective volume of distribution for the anesthetic. Although vagal blockade has been reported to increase HR in large animals like ponies (Derksen et al., 1981), the vagal blockade did not increase baseline HR significantly in rats in the present study. The differences in the effects of vagal blockade on HR may be a result of species difference in basal vagal nerve activity.

The autonomic nerves usually contain both afferent and efferent fibers. Hence the selective stimulation or recording of either the afferent or efferent nerve is essential to assess the role of the autonomic nerves in circulatory regulation. Vagal afferent fibers conduct the signals from most of the organs in the thoracic and abdominal cavity to the medulla, stimulating various viscerogenic reflexes. Continuous electrical stimulation of the afferent fibers may exert intensity-dependent inhibition of breathing, anxiety, or even painful behavioral reactions, often accompanying the increase in arterial pressure. As shown in Fig. 4, prior to nerve blockade, right vagal stimulation decreased HR and increased MAP, and the increase in MAP was not observed after blocking the portion proximal to the stimulation electrodes, suggesting that the increase in MAP before the proximal blockade could be attributed to vagal afferent activation. Combining vagal afferent blockade with vagal stimulation, we were able to selectively evaluate the role of the vagal efferent function in conscious rats (Li et al., 2003).

In conclusion, we have demonstrated a reversible blockade of the vagus nerve in conscious rats. A complete conduction block was achieved by local administration of a minimal dose of anesthetics. The reversible nerve blockade can be combined with nerve stimulation or nerve recording techniques to stimulate or record the efferent or afferent autonomic nerve activity in conscious animals. This technique, involving the use of a targeted delivery device, has the potential to aid in furthering our understanding of the role of the autonomic nervous system in cardiovascular regulation, and to promote physiological and behavioral studies.

Acknowledgements

This study was supported by a "Health and Labour Sciences Research Grant for Research on Advanced Medical Technology" from the Ministry of Health, Labour and Welfare of Japan,

"Health and Labour Sciences Research Grant for Research on Medical Devices for Analyzing, Supporting and Substituting the Function of Human Body" from the Ministry of Health, Labour and Welfare of Japan, "Program for Promotion of Fundamental Studies in Health Science" from the National Institute of Biomedical Innovation, a Grant provided by the Ichiro Kanehara Foundation, "Ground-based Research Announcement for Space Utilization" promoted by Japan Space Forum, and "Industrial Technology Research Grant Program in 03A47075" from New Energy and Industrial Technology Development Organization (NEDO) of Japan.

References

Borgdorff P, Versteeg PG. An implantable nerve cooler for the exercising dog. Eur J Appl Physiol Occup Physiol 1984;53(2):175–9.

Bowser-Riley F, Cornish M, Kidd C, Zheng F. Role of vagal afferent C fibres in the bradycardiac response to an increase in arterial blood pressure in ferrets. Exp Physiol 1990;75(6):859–62.

Costanzo EM, Barry JA, Ribchester RR. Co-regulation of synaptic efficacy at stable polyneuronally innervated neuromuscular junctions in reinnervated rat muscle. J Physiol 1999;521(Pt 2):365–74.

Cudd TA. Vagal blockade does not prevent adrenocorticotropin, cortisol, and cardiopulmonary responses to thromboxane A2. Can J Physiol Pharmacol 1998;76(12):1087–94.

Derksen FJ, Robinson NE, Stick JA. Technique for reversible vagal blockade in the standing conscious pony. Am J Vet Res 1981;42(3):523–5.

Gokin AP, Philip B, Strichartz GR. Preferential block of small myelinated sensory and motor fibers by lidocaine: in vivo electrophysiology in the rat sciatic nerve. Anesthesiology 2001;95(6):1441–54.

Kanje M, Lundborg G, Edstrom A. A new method for studies of the effects of locally applied drugs on peripheral nerve regeneration in vivo. Brain Res 1988;439(1–2):116–21.

Lee LY, Morton RF, Kou YR. Acute effects of cigarette smoke on breathing in rats: vagal and nonvagal mechanisms. J Appl Physiol 1990;68(3):955–61.

Li M, Zheng C, Kawada T, Sato T. Vagal stimulation improved acute-phase survival after myocardial infarction in conscious rats. Circulation 2003;108(Suppl. IV):IV-268, 1268.

Potocnik I, Tomsic M, Bajrovic F. Sensitivity of sensory axons to lidocaine nerve block in rats. Pflugers Arch 2001;442(6 Suppl. 1):R193–4.

Schultz HD, Gardner DG, Deschepper CF, Coleridge HM, Coleridge JC. Vagal C-fiber blockade abolishes sympathetic inhibition by atrial natriuretic factor. Am J Physiol 1988;255(1 Pt 2):R6–13.

Thalhammer JG, Vladimirova M, Bershadsky B, Strichartz GR. Neurologic evaluation of the rat during sciatic nerve block with lidocaine. Anesthesiology 1995;82(4):1013–25.

Vizek M, Frydrychova M, Houstek S, Palecek F. Effect of vagal cooling on lung functional residual capacity in rats with pneumonia. Bull Eur Physiopathol Respir 1983;19(1):23–6.

ELSEVIER

Cardiovascular Research 70 (2006) 457 – 465

Cardiovascular Research

www.elsevier.com/locate/cardiores

Targeted deletion of p53 prevents cardiac rupture after myocardial infarction in mice

Hidenori Matsusaka [a], Tomomi Ide [a], Shouji Matsushima [a], Masaki Ikeuchi [a], Toru Kubota [a], Kenji Sunagawa [a], Shintaro Kinugawa [b], Hiroyuki Tsutsui [b,*]

[a] *Department of Cardiovascular Medicine, Graduate School of Medical Sciences, Kyushu University, Fukuoka 812-8582, Japan*
[b] *Department of Cardiovascular Medicine, Hokkaido University Graduate School of Medicine, Kita-15, Nishi-7, Kita-ku, Sapporo 060-8638, Japan*

Received 10 August 2005; received in revised form 23 January 2006; accepted 1 February 2006
Available online 13 March 2006
Time for primary review 43 days

Abstract

Objective: Apoptosis may play an important role in cardiac remodeling after myocardial infarction (MI). p53 is a well-known proapoptotic factor. However, its pathophysiological significance in these conditions remains unclear. We thus examined the effects of target deletion of the p53 gene on post-MI hearts.
Methods: Anterior MI was created in male heterozygous p53-deficient ($p53^{+/-}$; $n=28$) mice and sibling wild-type ($p53^{+/+}$; $n=29$) mice by ligating the left coronary artery.
Results: By day 7, $p53^{+/-}$ mice had significantly better survival rate than $p53^{+/+}$ mice (89% vs. 69%, $P<0.05$). Notably, $p53^{+/-}$ mice had a significantly lower incidence of left ventricular (LV) rupture (7% vs. 28%, $P<0.05$) despite comparable infarct size (60±2% vs. 59±2%, P=NS), heart rate (488±15 vs. 489±17 bpm, P=NS), or mean arterial blood pressure (80±2 vs. 78±3 mm Hg, P=NS). The extent of infiltrating interstitial cells including macrophages into the post-MI hearts was not altered by the deletion of p53. Further, collagen deposition as well as the zymographic MMP-2 and -9 activities were comparable between $p53^{+/-}$ and $p53^{+/+}$ mice with MI. However, the $p53^{+/-}$ mice had a significantly thicker infarct wall. The number of TUNEL-positive cells in the infarct area was significantly lower in $p53^{+/-}$ mice than in $p53^{+/+}$ mice (423±86 vs. 1330±275/10^5 cells, $P<0.01$).
Conclusions: p53 is involved in cardiac rupture after MI, probably via the induction of a proapoptotic pathway. The inhibition of p53 may be a potentially useful therapeutic strategy to manage post-MI patients.
© 2006 European Society of Cardiology. Published by Elsevier B.V. All rights reserved.

Keywords: Apoptosis; Extracellular matrix; Infarction; Myocytes; Remodeling

This article is referred to in the Editorial by M.T. Crow (pages 401–403) in this issue.

1. Introduction

Myocardial infarction (MI) leads to complex structural alterations (remodeling) involving both the infarcted and noninfarcted left ventricular (LV) myocardium [1]. Early remodeling, which occurs during the early phase of MI, is characteristic for LV wall thinning and cavity dilatation in the infarct region (infarct expansion). Cardiac rupture is a lethal complication accounting for 5–30% of in-hospital mortality of MI [2] and is often associated with a transmural infarction, no prior history of angina pectoris, and a relatively large Q-wave infarct. Although the significance of these factors remains unestablished, accumulated lines of evidence have suggested that cardiac rupture results from the continuous stretch of infarcted and structurally weakened myocardium [3]. Recently, inflammatory cell infiltration and activation of matrix metalloproteinases (MMPs) have also been implicated in the pathogenesis of cardiac rupture [4,5].

* Corresponding author. Tel.: +81 11 706 6970; fax: +81 11 706 7874.
E-mail address: htsutsui@med.hokudai.ac.jp (H. Tsutsui).

0008-6363/$ - see front matter © 2006 European Society of Cardiology. Published by Elsevier B.V. All rights reserved.
doi:10.1016/j.cardiores.2006.02.001

The tumor suppressor gene p53 is an important transcription factor regulating cell death and proliferation. It induces apoptosis in response to a variety of stresses such as ischemia [6,7]. In fact, there is evidence supporting that p53 is activated in the ischemic hearts [8] and apoptotic myocytes are detected in the infarcted and border zone regions during the early days of MI [9,10]. Based on these lines of evidence, we postulated that p53-dependent apoptosis might play an important role in early LV rupture after MI. However, no previous studies have yet determined the pathophysiological significance of p53 in this deleterious process. In the present study, we evaluated the effects of a targeted deletion of the p53 gene on the development of cardiac apoptosis and rupture after experimental MI in mice. To ensure selective and long-term complete inhibition of p53, we employed p53 knockout mice [11] because the most effective way to obtain the direct evidence for a role of p53 is through gene manipulation. We demonstrated that p53 was involved in cardiac rupture after MI, probably via the induction of proapoptotic pathway. The inhibition of p53 may be a potentially useful therapeutic strategy to manage post-MI patients.

2. Methods

2.1. Animals

The study was approved by our Institutional Animal Research Committee and conformed with the *Guide for the Care and Use of Laboratory Animals* published by the US National Institutes of Health (NIH Publication No. 85-23, revised 1996). We used the progeny of homozygous p53 deficient mice ($p53^{-/-}$), heterozygous p53 deficient mice ($p53^{+/-}$), and their wild-type littermates ($p53^{+/+}$, C57BL/6J) ranging in age from 10 to 14 weeks old. $p53^{-/-}$ and $p53^{+/-}$ mice are viable, fertile, and indistinguishable from $p53^{+/+}$ mice in appearance but are prone to the spontaneous development of a variety of tumors by 6 months of age [12]. We thus assessed mice at the age of 10 to 14 weeks old for comparison between groups. The original breeding pairs used to develop the mice for this study were obtained from Jackson Laboratories (Bar Harbor, Maine). Genotypes of the mice were determined by PCR analyses of the mouse tail DNAs [13]. For p53, we used a sense oligonucleotide primer (5′-CCCGAGTATCTGGAAGACAG-3′) and an antisense primer (5′-ATAGGTCGGCGGTTCAT-3′). For the neomycin cassette, we also used a sense oligonucleotide primer (5′-CTTGGGTGGAGAGGCTATTC-3′) and an antisense primer (5′-AGGTGAGATGACAGGAGATC-3′). The amplicon from the WT allele is 600 bp, and the mutant allele is 280 bp (Fig. 1).

2.2. Creation of MI

We created MI in male $p53^{-/-}$ ($p53^{-/-}$+MI), $p53^{+/-}$ ($p53^{+/-}$+MI), and sibling wild-type mice ($p53^{+/+}$+MI) by ligating the left coronary artery [14]. A sham operation without coronary artery ligation was also performed in both $p53^{+/+}$ ($p53^{+/+}$+Sham) and $p53^{+/-}$ ($p53^{+/-}$+Sham) mice.

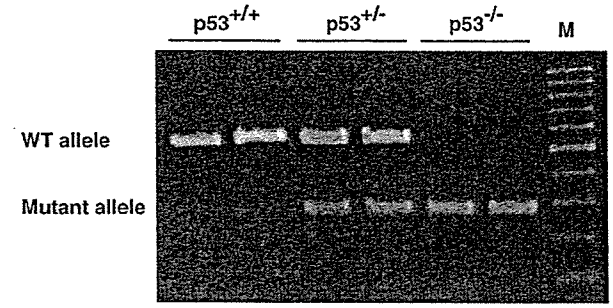

Fig. 1. PCR genotyping of $p53^{+/+}$, $p53^{+/-}$, and $p53^{-/-}$ mice. The amplicon from the WT allele is 600 bp, and the mutant allele is 280 bp. M, marker.

2.3. Experimental protocol 1: 7-day post-MI study

2.3.1. Survival

A survival analysis was performed for the $p53^{+/+}$+MI (n=29), $p53^{+/-}$+MI (n=28), and $p53^{-/-}$+MI (n=20) mice. During the 7-day study period, the cages were inspected daily to identify any deceased animals. All deceased mice were examined for the presence of MI as well as pleural effusion and cardiac rupture, based on a diagnosis of the presence of a blood clot within the chest cavity in the postmortem examination.

2.4. Experimental protocol 2: 3-day post-MI study

Because a substantial portion of the MI animals died within 7 days after MI, in vivo LV function and myocardial histopathology were also evaluated in a separate group of additional $p53^{-/-}$ ($p53^{-/-}$+MI), $p53^{+/-}$ ($p53^{+/-}$+MI), and sibling wild-type mice ($p53^{+/+}$+MI) at 3 days of surgery treated identically to experimental protocol 1. A sham operation without coronary artery ligation was also performed in both $p53^{+/+}$ ($p53^{+/+}$+Sham) and $p53^{+/-}$ ($p53^{+/-}$+Sham) mice. The numbers of $p53^{-/-}$ mice were less than those of $p53^{+/-}$ mice because of the limited number of $p53^{-/-}$ mice available for the detailed subsequent analysis. In fact, the previous study has shown that a significant proportion of female $p53^{-/-}$ mice die during embryogenesis or in the period between birth and weaning [15]. In addition, in $p53^{-/-}$ female embryos, the normal process of neural tube closure failed, leading to exencephaly and subsequent anencephaly. Another possible explanation for the lower availability of $p53^{-/-}$ mice is that p53 is involved in the normal process of spermatogenesis [16].

2.4.1. Echocardiographic and hemodynamic measurements

Echocardiographic studies were performed under light anesthesia with tribromoethanol/amylene hydrate (Avertin; 2.5% wt./vol., 8 μL/g ip) and spontaneous respiration [14]. A

two-dimensional parasternal short-axis view of the LV was obtained at the level of the papillary muscles. In general, the best views were obtained with the transducer lightly applied to the mid upper left anterior chest wall. The transducer was then gently moved cephalad or caudad and angulated until desirable images were obtained. After confirming that the imaging was on axis (based on roundness of the LV cavity), two-dimensional targeted M-mode tracings were recorded at a paper speed of 50 mm/s. Next, a 1.4 Fr micromanometer-tipped catheter (Millar) was inserted into the right carotid artery and then was advanced into the left ventricle to measure the LV pressures. One subset of two investigators, who were not informed of the experimental groups, performed in vivo LV function studies. Our recent validation study has shown that the intraobserver and interobserver variabilities of our echocardiographic measurements for LV cavity dimensions and fractional shortening were small and measurements made in the same animals on separate days were highly reproducible [14].

2.4.2. Infarct size and wall thickness

Infarct size was determined by the methods described in rats [17] and also in mice [18,19]. The heart was excised and the right and left ventricles including the septum were dissected. The left ventricles were cut from apex to base into 3 transverse sections. Five-μm sections were cut and stained with Masson's trichrome. Infarct length was measured along the endo- and epicardial surfaces from each of the LV sections, and the values from all specimens were summed. Total LV circumference was calculated as the sum of endo- and epicardial segment lengths from all LV sections. Infarct size (in percent) was calculated as total infarct circumference divided by total LV circumference. In our preliminary study, we confirmed excellent reliability of infarct size measurements, in which a morphometric methodology similar to that used in this study was employed. The intraobserver and interobserver variabilities between two measurements divided by the mean of the two measurements, expressed as a percentage, were less than 5%. Therefore, our technique could be considered to allow reliable assessment of infarct size in mice.

To further evaluate the effects of p53 on the risk area and infarct size, a separate group of animals including $p53^{+/-}$+MI ($n=5$) and $p53^{+/+}$+MI ($n=5$) was created. After 24 h, Evans blue dye (1%) was perfused into the aorta and coronary arteries with distribution throughout the LV wall proximal to the site of coronary artery ligation. The nonischemic area was stained blue. Hearts were excised and sliced into cross-sections below the ligature. These sections were weighed and then incubated with a 1% triphenyltetrazolium chloride (TTC) solution at 37 °C for 20 min. The infarct area (pale), the area at risk (not blue), and the total LV area from each section were measured, multiplied by the weight of the section, and then totaled from all sections [20].

To quantitate wall thinning, the thickness of the infarct wall was determined using the leading-edge method at the thinnest point of transmural infarction. The noninfarct wall measurement was then acquired from the same slide at the point on the LV diametrically opposed to the point used for infarct thinning. The wall thinning was calculated by dividing the infarct wall thickness by the noninfarct wall thickness [21, 22].

2.4.3. Myocardial histopathology

From the mid-LV transverse sections, 5-μm sections were cut and stained with hematoxylin and eosin and Masson's trichrome. To quantify myocardial infiltrates, nuclear density (nuclei per square millimeter) was determined. In each animal, 5 independent high-powered fields were analyzed. To further determine the number of macrophages, an immunohistochemical analysis using a specific antibody against mouse Mac-3 (BD Pharmingen) was performed.

The collagen volume fraction was determined by the quantitative morphometry of Masson's trichrome-stained mid-LV sections. Interstitial collagens were also stained with Sirius red.

2.4.4. MMP zymography

Zymographic MMP levels including MMP-2 and MMP-9 were determined in the infarcted LV using gelatin zymography [23].

2.4.5. Apoptosis

To detect apoptosis, LV tissue sections were stained with terminal deoxynucleotidyl transferase-mediated dUTP nick end-labeling (TUNEL) staining (TaKaRa). The number of TUNEL-positive nuclei was counted in the infarcted and border zone LV, and the data were normalized per 10^5 total nuclei identified by hematoxylin-positive staining in the same sections. We further examined whether apoptosis is present by the more sensitive ligation-mediated PCR fragmentation assays (Maxim Biotech Inc.).

2.4.6. Akt protein

The Akt protein levels were analyzed in cardiac tissue homogenates by Western blot analysis with a polyclonal

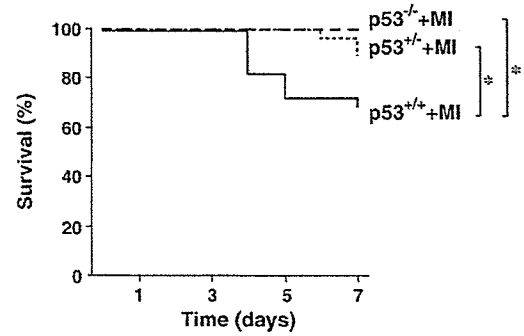

Fig. 2. Kaplan–Meier analysis of survival after MI in $p53^{+/+}$+MI ($n=29$), and $p53^{+/-}$+MI ($n=28$), and $p53^{-/-}$+MI ($n=20$) mice. There was no death after the sham operation in $p53^{+/+}$ and $p53^{+/-}$ mice (data not shown). *$P<0.05$ for difference from the $p53^{+/+}$+MI.